# INVESTIGATION ON STRETCH FORMABILITY OF AA6023-T6 ALLOY SHEET

A thesis submitted

by


**Manaye Mathewos Handiso**

**(GSR/0091/09)**


For the Partial fulfilment of the

Requirement for the award of degree

of

Master of Science

**in Manufacturing Engineering**

Under the Supervision & Guidance of

**Dr. G. Somasundaram (PhD)**

Professor

**Dr. Perumalla Janaki Ramulu (PhD)**

Associate Professor


**Mechanical Design & Manufacturing Engineering Program**

**School of Mechanical, Chemical and Materials Engineering**

**Adama Science and Technology University**

Adama, Ethiopia


June 2018

**ADAMA SCIENCE AND TECHNOLOGY UNIVERSITY**

**School of Mechanical Chemical and Material Engineering**

**Program of Mechanical Design and Manufacturing Engineering**


# INVESTIGATION ON STRETCH FORMABILITY OF AA6023-T6 ALLOY SHEET


By

**Manaye Mathewos Handiso (GSR/0091/09)**


**Approved by Board of Examines**

Approved by Board of Examiners

| | | |
|---|---|---|
| ______________________ | _________ | _________ |
| Chairman, Department Graduate Committee | Signature | Date |
| ______________________ | _________ | _________ |
| Major Advisor | Signature | Date |
| ______________________ | _________ | _________ |
| Co-Advisor | Signature | Date |
| ______________________ | _________ | _________ |
| Internal Examiner | Signature | Date |
| ______________________ | _________ | _________ |
| External Examiner | Signature | Date |

# Candidate Declarations

I hereby declare that the work which is being presented in this thesis entitled **"Investigation on stretch formability of AA6023-T6 alloy sheet''** in partial fulfilment of the requirements for the award of the degree of masters of science in Manufacturing Engineering is an authentic record of my own work carried out **September to Jun 2017** under the supervision of **Dr. G. Somasundram**, and **Dr. Perumalla Janaki Ramulu**, Program of Mechanical Design and Manufacturing Engineering, Adama science and Technology University, Ethiopia.

The matter embodied in this thesis has not been submitted by me for the award of any other degree or diploma. All relevant resources of information used in this thesis have been duly acknowledged.

| | | |
|---|---|---|
| Manaye Mathewos Handiso | _________________ | ______________ |
| Candidate | Signature | Date |

This is to certify that the above declaration made by the candidate is correct to the best of my knowledge and belief. This thesis has been submitted for examination with our approval.

| | | |
|---|---|---|
| Dr.Somasundaram | ________________ | ______________ |
| Advisor | Signature | Date |
| | | |
| Dr. P. Janaki Ramulu | _________________ | ______________ |
| Co-Advisor | Signature | Date |

# Acknowledge

While bringing out this thesis to its final form, I came across a number of people whose contributions in various ways helped my field of research and they deserve special thanks. It is a pleasure to convey my gratitude to all of them.

I would like to express a sincere and special thanks to my Advisor **Dr. G. Somasundram** for his continuous support, guidance, creative ideas, through correction and suggestions greatly contributed in doing this thesis. Without his courage and patience this would not been possible.

I would like to express my deepest gratitude to my co-advisor, **Dr. P. Janaki Ramulu**, for his guidance and support. His extreme energy, creativity and excellent skills have always been a constant source of motivation for me. The perfection that he brings to each and every piece of work that he does always inspired me to do things right at first time. His involvement with originality has triggered and nourished my intellectual maturity that will help me for a long time to come. I am proud to record that I had the opportunity to work with an exceptionally experienced professor like him. He is a great person and one of the best mentors, I always is thankful to him.

I am also grateful to **Mr.Abdulmalik**, **Program Chair,** Mechanical Design and Manufacturing Engineering Program and also member of the Post-Graduate Committee in the School of Mechanical Chemical, Material and Chemical Engineering, for their support and contribution to the success of my thesis work.

I would like to thank Lab assistant at Adama Science and Technology University Mechanical Engineering department, **Mr. Yilikal Dinkayehu** for his support during experimental works.

I am deeply indebted to the Lab Assistant at Ethiopian Conformity Assessment Enterprise, **Daniel Ketema**, who helped me for conducting the experiments.

Thank you to all my colleagues and friends of Manufacturing Engineering stream, who supported me in all possible forms. In particular, special thanks go to **Dereje, Geletu Mentemo**, and **Anjelo Lidetu**, I am very grateful.

I would like to thank my family. The constant inspiration and guidance kept me focused and motivated. My greatest regards to my mother **Arese Ergena** she always courage me to face the complexities of life and complete this project successfully.

Above all, I extend my special thanks to the Almighty God for his mercy on me and without his help and courage I am nothing to do anything.

# Abstract

*Sheet metal forming is a process widely used in the manufacturing industry. There are several sheet metal forming processes are existed including stretch forming process. In this thesis, stretch formability of AA6023-T6 alloy sheet at room temperature and annealed sheet at 400$^0$C has been performed. For which mechanical properties were evaluated through tensile test for all the conditions of AA6023-T6 sheet. Also, microstructure and material hardness tests were conducted by using Optical microscope and Vickers hardness (VHR) test respectively. The results of microstructure show, refined microstructure for annealed sheets at 400$^0$C compared to sheet at room temperature. Annealing process caused reduction in material hardiness, which is acceptable value for sheets for different applications. For stretching operations, simulations were performed using limit dome height (LDH) test using PAM STAMP 2G software. During LDH test, the maximum value of LDH for annealed sheets of AA6023-T6 at 400$^0$C and minimum value for sheets at room temperature is observed. Uniform thickness distribution for annealed blanks at 400$^0$C is observed compared to room temperature. The room temperature stretch formability of AA6023-T6 alloy sheet has 39.5 maximum dome height and annealed sheet at 400$^0$C has 43 maximum dome heights. By which, annealed AA6023-T6 alloy sheet has good stretch formability.*



**Keywords***: Mechanical properties; formability; forming limit diagram; limit dome height; thickness distribution; microstructure and materials hardness.*

# Table of contents

# List of Tables

# List of Figures

# List of Symbols

| | |
|---|---|
| ***FLD*** | *Form Limit Diagram* |
| ***ULC*** | *Upper Limit Curve* |
| ***LLC*** | *Lower Limit Curve* |
| ***FFL*** | *Fracture Form Limit* |
| ***LDH*** | *Limit Dome Height* |
| ***CAD*** | *Computer Aided Design* |
| ***FE*** | *Finite Element* |
| ***RD*** | *Rolling Direction* |
| ***LD*** | *Longitudinal Direction* |
| ***TD*** | *Transvers Direction* |
| ***UTS*** | *Ultimate tensile strength* |
| ***UE*** | *Uniform elongations* |
| ***YS*** | *Yield strength* |

# List of acronyms

| | |
|---|---|
| $r$ | *Anisotropy factor* |
| $n$ | *Work hardening exponent* |
| $m$ | *Strain rate sensitivity* |
| $k$ | *Materials strength coefficient* |
| $e$ | *Engineering strain* |
| $s$ | *Engineering stress* |
| $\Delta L$ | *Change in length* |
| $L$ | *Original gauge length* |
| $\boldsymbol{\varepsilon}$ | *True strain* |
| $\sigma$ | *True stress* |
| $\tau$ | *Shear stress* |
| $\bar{\sigma}$ | *Equivalent stress* |
| $\varepsilon_w$ | *True width strain* |
| $\varepsilon_t$ | *True thickness strain* |
| $w_f$ | *Final width* |
| $w_o$ | *Original width* |
| $t_f$ | *Final thickness* |
| $t_o$ | *Original thickness* |

# CHAPTER 1

## 1.1 Introduction

Sheet metal forming is a process widely used in the manufacturing industry. There are several sheet metal forming processes are identified including stretch forming process. In stretch forming process the sheet metal is clamped around its edge and stretched over a die or forming block, which moves up ward, downward or sideways, depend up on the particular machine. Stretch forming is used primarily to make aircraft-wing skin panel, automotive doors panel and window frames etc. The design of components needs the analysis of instability and determining of possible deformation of sheet metal. The determination of possible forming limits and analysis of instability of sheet metal is predicted from forming limit diagrams (FLDs) [1]. Stretch formability is one sheet metal forming process in which force is applied on sheet metal to modify its shape and geometry without removing or cutting of material [2]. The applied load on sheet metal causes the plastic deformation when it is greater than yield strength of the metal. The stress induced during the process are greater than yield strength, but less than fracture strength of the material [3]. Mechanical behaviour of sheet metal is important to understand when manufacturing sheet metals products. Generally, a desirable property for metals is a large plastic deformation before necking. When necking of the metals occurs, diffuse necking is preferred over localized necking. A high total elongation of the metal before fracture is also desirable for sheet metal forming. Some metal such as a low carbon steels and aluminium-magnesium alloy may experience yield point elongation. Grain size, structure and orientation also important in a sheet metal workpiece. Grain will affect the properties as well as surface finish [4]. Another important factor which has influence on sheet metal forming is anisotropy. It is the directional variation of mechanical properties. In other words, the reaction of a materials to applied stress at different direction has different reaction to the applied stress. The strength and formability of the materials are the main properties which are very important for industrial applications of sheet metals [5, 6]. The forming behaviour of a certain sheet metals always depend up on the forming temperature during forming process. For instant, aluminium series of 6xxx alloys has quite less level of formability at room temperature than aluminium series of 5xxx alloys because of its strength [7].

This study is mainly targeted on the determination of stretch forming behaviour of AA6023-T6 sheet because, many recent automotive, ship, train body and aerospace industries are using aluminium alloy widely in order to achieve the requirements of lightweight and suitable formability of different parts [8].

## 1.2 Statement of the problem

Sheet metal forming industries use the stretch forming process of sheet metals for the application areas like: aerospace, shipping, air crafts, and automotive parts. For these application areas, the requirement of good stretch formability is primary consideration. The stretch formability of aluminium alloy sheet affected by forming parameter like:

- Forming temperature
- Forming speed
- Punch force
- Lubrication (coefficient of friction)
- Mechanical properties of the sheet metals

Forming temperature has significant effect on stretch formability. Stretch formability of aluminium alloy sheet at room temperature has less formability than elevated temperature. But forming process at elevated temperature causes the excessive ductility on sheets. To overcome these problem annealing process of sheet metal is necessary in stretch formability of aluminium alloy sheet.

## 1.3 Objective of the study

### 1.3.1 General objective

The general objective of this thesis is examining the stretch formability of AA6023-T6 alloy sheet at room temperature and annealed at 400$^{o}$C.

### 1.3.2 Specific objectives

The specific objectives of the project are:

- Investigating the mechanical properties of AA6023-T6 alloy sheet at room temperature and annealed sheet at 400$^{0}$C at different three rolling directions (0$^{0}$, 45$^{0}$,90$^{0}$)
- Evaluating the plastic anisotropy of AA6023-T6 alloy sheet at room temperature and annealed sheet at 400$^{0}$C at different three rolling directions (0$^{0}$, 45$^{0}$,90$^{0}$)
- Modeling and simulating stretch forming using limit dome height test on different strain paths.
- Developing the forming limit diagrams for all three rolling directions and at two different heating conditions

## 1.4 Aim and scope of the study

Sheet metal forming process vary from simple to complex. For instant, bending occurs at one end of the spectrum, in the middle stretch forming and at the other end deep drawing takes place. Regarding of forming process, the mechanical properties of sheet material has great influence on formability, which is a measure of the amount of deformation a material can withstand before excessive thinning or fracture occurs. Determining how much a material can deform is necessary for forming operations. Fracture is caused by excessive punch load, excessive blank holder force, excessive friction between punch and die and insufficient radius of die and punch. In this thesis the stretch formability of AA6023-T6 sheet metal was simulated along with mechanical property and plastic strain ratio testes were evaluated experimentally. The properties evaluated from the experiments of tensile test and plastic strain ratio testes are used as the input parameters for simulation of stretch formability of sheet metal by using finite element simulation. The study is initiated by preparing samples for tensile and plastic strain ratio tests. The sheet metal forming parameters namely, strain hardening exponent (n), the material strength coefficient (K), and plastic strain ratio (r) are evaluated. The simulation process was performed in finite element code using (LDH) test in to finite element code. The materials properties, the dimensions of blank, different process parameters and other criteria considered for simulation are given in chapter three. Forming limit diagram (FLD), distribution of thickness and dome height are evaluated simulation for all conditions of experimental results. From overall analysis of the results a good formability condition of AA6023-T6 sheet metal was suggested.

## 1.5 Significance of the study

The applications of aluminum alloy, in automotive industry, aerospace, marine and ship-building industry and aircrafts parts like: aircraft skins, cowls, and airframe components depends stretch formability process. The stretch formability of aluminum alloy sheets depend upon the mechanical properties, forming conditions cold forming or hot forming, along with other forming factors. The evaluation of stretch formability based on these parameters is important for industrial applications. Aluminum sheet alloys with potential application as light weight automotive body panels are formed by stretch forming process. One of the main requirements of the modern automotive industries are quality in stretch formability of aluminum alloy. This study helps the modern industries to achieve a good stretch formability on one of aluminum alloys sheet.

## 1.6 Organization of the study

This thesis contains five chapters. In the first chapter the general information about the stretch formability process and outline of the present study was given. The second chapter is literature review based on previous studies related to the stretch formability. The review of studies consists of the experimental results, numerical simulation and the effect of different parameters. Within this chapter the concept of the formability and its relation with various parameters from the previous studies are briefly explained. In third chapter, the specification of material and different methodology used in this study are mentioned. The methods used in this chapter contains the heat treatment of sheet metal, tensile testing process, plastic strain ration analysis, the stress – strain relationship, strain hardening process and Hill yield criterion. In the last numerical simulation details are explained. Fourth chapter focuses on the presentation of results obtained from both experiment and numerical simulation analysis. Fifth chapter deals with the major conclusion of the present work as well as suggestion for future possible developments in this area.

# CHAPTER 2

## LITERATURE REVIEW

### 2.1 Introduction

Formability of a given sheet metal indicated the ability of the sheet metal to be formed under different forming conditions to different sizes and dimensions [9]. The amount of strain hardening in the material decided the formability of the materials. The tensile test was one of the mechanical properties evaluation process in which the strain hardening exponent of the sheet metal evaluated. If the tensile tests of the sheet metal had maximum percentage of elongations, it can be predicted as the sheet metal with a good formability [10]. Formability of sheet metal also depends on the property of material determined from tension tests, such as tensile strength, yield strength, percentage elongation and the uniform elongation. These material properties are not sufficient to describe the sheet metals behavior deformation. The characteristics are, however, important to sort out unsuitable sheet metals. Although elongation after fracture and uniform elongation describe the suitability of sheet metals for forming process approximately, these values determined from tension test or uniaxial loading may not be sufficient to determine the suitability of sheet metal for deformation process since the stress condition may be different.

### 2.2 Influence of forming temperature

Forming temperature has significant influence on formability. Many researches were developed on the effect of temperature on the formability of different sheet metals. For example, Nolan *et al.*(2009) [11] studied the formability of a 7000 series alloy under different forming temperature. They performed the tensile tests and deep drawing tests to evaluate the forming behaviour. The experiment was taken at both elevated and room temperature. In the drawing process of the metal, the formability of the given sheet metal increased with the increase of forming temperature. This warm forming behaviour of the sheet metal indicated that the condition of formability of the alloy improved with that of the forming temperature. For the warm forming condition of 7000 series alloy in general the forming temperature observed in the range of 200◦C to 600◦C. The forming condition of stretch flange has a good formability at warm forming condition than cold forming process. Tokita *et al.* (2017) [12] studied the forming conditions of the stretch formability of two different high strength steels. The forming was preferred on warm forming by spherical stretch forming tests at various forming temperature including room temperature up to 600$^{c}$C. Their experiment showed the suitable forming temperature for stretch formability of steels. The observations from the experiments indicated the value of maximum dome height related to the maximum formability indications. There was maximum dome height for test of steel at elevate temperature and minimum dome height at room temperature forming process. High initial forming temperature was one of the affecting factor which causes the loss of quality in the forming process and also the coefficient of friction has a significant influence on the forming behaviour of the alloy. Ali and Jumah (2012) [13] investigated the forming behaviour of annealed aluminium alloy at different forming temperature. The formability of alloy increased with the increasing of the forming temperature. The comparison between forming process in a moderated forming temperature and forming process after annealing was observed. The result indicates that there is acceptable formability for alloy which was formed at moderated forming temperature than the alloy which was formed after annealing process. Also there is much more strength for alloy which was formed at moderated temperature than the alloy after annealed. In case of warm forming condition, the increase of temperature got significant effect on formability of sheet metals [14, 15]. When the forming temperature increase the stress required to form the 7000-aluminium alloy specimen decreased. At given forming temperature which was less than $150^0$C the formability of alloy minimum because of the stress concentration and when the forming temperature increased to $300^0$C, the formability of the alloy increased. There was poor formability of 7000- aluminum alloy at room temperature compared to from $150^0$C forming temperature to $475^0$C forming temperature [16]. When temperature was at maximum level, the formability was significantly good but the drawback at this forming temperature was the excessive ductility. In this case the application of alloy limited to its strength. In general, elongation increased, with increase of temperature of AA6061-T6 alloy during tension test. Moreover, at elevated temperature greater or equal to $280^0$C, the elongation increase with decreasing strain rate. With spreading of the deformation area, the deformation was more uniform than that at high strain rate; elongation increase gradually [17]. From tensile test, the true stress – true strain relationship showed that high strength alloy AA7075 has maximum ultimate strength and minimum total elongation at room temperature. During tensile test, there was no well-defined changes at forming temperature of $60^0$C or $100^0$C. However, there was lowering in elongation at forming temperature ranging from $140^0$C to $220^0$C. When the temperature is $260^0$C, the strength of the alloy decreases significantly as well as total elongation. It showed that the maximum forming temperature was significant change in mechanical property of alloy. At warm forming of AA7075 alloy the materials strain rate hardening exponent was an important property to indicate the formability characteristics of alloy. The stress – strain relationship of the alloy showed that work hardening at maximum temperature decreases significantly with an increase of forming temperature from $140^0$C to $220^0$C [18].

For AA5182 alloy given strain rate, with an increase in the temperature causes decrease in strength and increase in ductility. Similarly at a given temperature, the increase in strain rate, both yield strength and ultimate tensile strength decrease and ductility increased. At the range of forming temperature from $200^0$C to $300^0$C the properties of strain hardening of the alloy was maximum. Also at $300^0$C, strain hardening was lower and almost negligible at the lowest strain rate. The value of strain hardening had inverse proportionality to the forming temperature, i.e. increase in forming temperature causes decrease in strain hardening. The influence of strain rate was visible in the flow of stress. The total elongation depended on strain rate sensitivity index value, when the alloy had larger strain rate sensitivity index value and also higher total elongation. The alloy was more than 100% total elongations at $250^0$C and $300^0$C and the maximum elongation of 148% obtained at the highest temperature and lowest strain rate. The stretch formability of aluminum alloys with series of 6000 and 7000 were low at room temperature forming condition than hot forming condition. Aluminum alloys with 5000 series, had the largest formability range even at room temperature. Also the lowest strength related to aluminum alloys series of 6000 and 7000. Forming behaviour of aluminum alloy increase with the increase of forming temperature either it is warm forming or hot forming temperature. Aluminum alloy with series of 7000 also had a good stretch formability at elevated temperature. In addition that the percentage of copper content in aluminum alloy was a significant effect on formability of alloy [19].

## 2.3 Influence of strain and plastic anisotropy on stretch formability

The increase or reduction of strain and plastic anisotropies related to texture intensity and texture distribution should be the main factors for good stretch formability. Refining strain（ductility）of the materials also influence the stretch formability [20-24]. The materilas texture intensity has effect on stretch formability. Stretch formability of AZ31 Mg alloy sheet was evaluated at room temperature. And results from expermental tests indicats that, lower r- value and higgher n- value showed exellent stretch formability [25].

## 2.4 Forming limit diagram

The forming limit diagram (FLD), was introduced by Keeler [26] and Goodwin [27]. Forming limit diagram (FLD) is used to predict the materials formability behaviour under different forming condition. It played a great role in industries, because it was also the most applicable method to evaluate the formability of sheet metals [28-34]. Forming limit diagrams were used to determine the forming strain during forming process. The value of the work- hardening coefficient (n) and the anisotropy factor (r) also determined from tension test permit prediction approximately the maximum possible strain achievable in deep-drawing and stretch forming operation [35]. The prediction of fracture formation of a certain metal in the forming process is one of the main criteria for analysing a suitable sheet metal forming process in order to achieve a good formability. The prediction of fracture forming limit highly depends on the forming temperature of the forming process [36 - 40].

Sivanadini, *et al.* (2009) [37] studied the forming behaviour of magnesium alloys. Magnesium alloys of aluminium are used in many recent industries due to their lightweight and suitable strength. Also had good formability on the condition of hot forming process. The forming process of Magnesium alloys  at room temperature causes less formability than the forming process at hot forming temperature, because, of the ductility of the alloy. If the ductility of the Magnesium alloy increased the formability of the alloy also increase. Since, the increase in ductility of the Magnesium alloy predicts the formability behaviour Magnesium alloy sheets.

The forming limit diagram is also the forming limit curve, which is one of necessary value during practical assessment of sheet stretch forming process. The parameters such as, strain hardening exponent (n), strain rate sensitivity exponent (m), the anisotropy strain rate (r) play a significant role in stretch formability of sheet metal [41]. The value for these parameters calculated with respect to the specimen just before fracture. Forming limit diagrams (FLDs) are a suitable and often used mechanism for classification of the formability and investigation of sheet metal forming process. Forming limit diagram (FLD) also used to indicate the forming limit of a given sheet metals at different state of deformation. For different materials the upper limit curve (ULC) of the forming limit diagram provides breaking, and they calculated with respect to specimens just before breaking. This result was presented at upper limit curve (ULC) of forming limit diagram (FLD) shown in Fig 2.1. The increase in local necking causes the increase in in deformation of a certain specimen at stress concentration area. While the local necking increased further there was no change in stress to the rest of part of the specimen which was not subjected to the necking. Start a local neck lies directly above the cloud strain states of or above the lower limit curve (LLC), represent in the Fig 2.1 [42, 43].

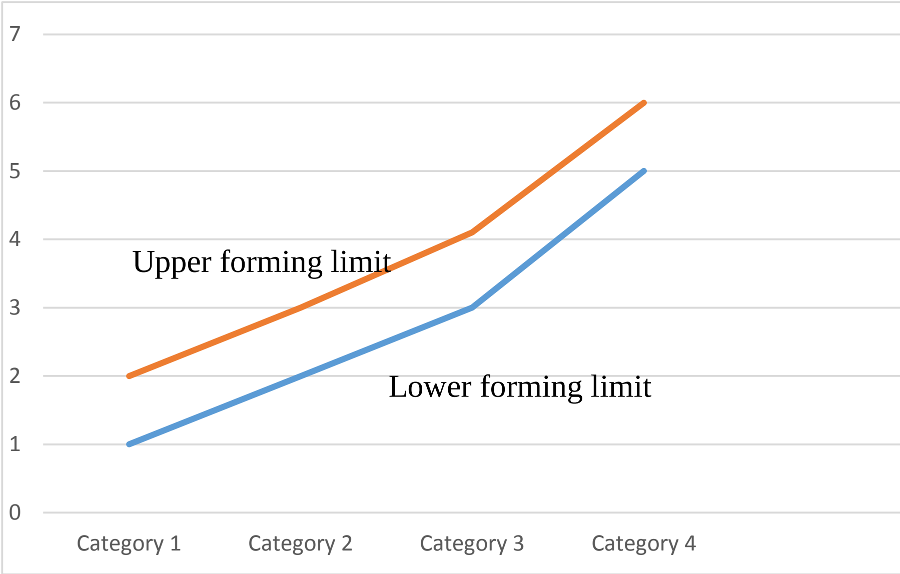


***Figure 2.1 Schematic representation of Forming limit diagram***

The deformation force influences the determination of forming limit diagram (FLD). The loss of stability in tensile strength was considered during determination of form limit diagram. The loss of stability in tensile strength was considered during deformation process. From the forming limit diagram (FLD) the direction of thickness distribution depends on the plastic deformation of the sheet metal. When the stretching of the sheet metal occurs the sheet start to the thinning in the direction of major strain direction. That means the left part of mentioned form limit diagram [44]. From forming limit diagrams (FLDs) of the major and the minor strain, the stretch formability of sheet metals indicate the forming behaviour of a metal. The materials strain hardening exponent (r) value has significant effect of the forming limit diagram. The strain hardening exponent value of steel sheet were evaluated with forming limit diagram. The results obtained from true uniform strain in tensile test agreed with the forming limit diagram (FLD) obtained at room temperature, $150^0$C and $450^0$C. The experimental value of uniaxial tensile test at temperature of $150^0$C and $450^0$C indicated the formability behaviour of the steel sheet. At plain strain condition the effect of temperature on forming limit diagram indicate the level of forming limit diagram. The levels of forming limit diagram decreased with the increase of sheet metal temperature. At $450^0$C temperature the forming limit curve got maximum level which was observed from the experiment. The increase in forming limit diagram (FLD) indicate the further increase of forming temperature was effect of sensitivity index. There was increase in strength, material strength coefficient and relative increase in strain hardening exponent at $450^0$C. From forming limit diagrams, the strain data points in the neck and also in the fracture region, there was down ward trend points in these data points toward biaxial stress line, because of the increased in forming temperature. The increase in forming temperature caused the decrease in mean flow stresses. Since, there was less mean flow stresses of sheet metal it required the minimum deformation load. The comparison between the sheet metal's temperatures of $300^0$C and $450^0$C indicated there was slightly increase in the load at $450^0$C [45]. Sheet metal forming process limited by plastic instability that occurs in forming metal in the form of diffused necking followed by localized necking and as well as final failure. The materials properties like, strain rate sensitivity parameter (m), stain hardness exponent (n), the anisotropy parameter (r), the grain size and as well as strain path have great role in determination of forming limit diagram (FLD). Since the actual strain path do not have a good agreement with the experiments [46].

There are many studies were involved on the formability behaviour and forming limit diagram (FLD) behaviour of the materials. Palmeth *et al*. (2013) [47] studied the stretch formability behaviour of H240LA steel sheets and observed that FLD behaviour of steel sheet which defines formability under different state of deformation. The necking limit strain (FLC, forming limit curve) indicates the materials stretch forming status before fracture.

Kang *et al.*(2009) [48] studied the relationship between the stretch formability and work hardening of Mg alloy at room temperature. In his study, he observed that the linear relationship between stretch formability and work-hardening capacity, represented by the invers of yield ratio.

Holmberg *et al.* (2004) [49] observed the forming limit properties of sheet metal. The forming limit in plane was determined by developing a test procedure. The tests were carried out in a tensile testing machine. The specimen shape and the forces arrangements were essential in order to get successful tests. The study involves both the numerical and experimental work. The appropriate specimen design was found by performing simulations. Mild steel and High strength steel were included in the study. The accuracy of the simulations depends on the quality of the material properties given as input to the simulations. Material properties for sheet metal forming are stress-strain relations describing the work-hardening of the material and forming limits are of main interest. A test procedure for determining the complete left-hand side of FLC by tensile tests was outlined. By altering the geometry of the specimen, different strain conditions are achieved. The right-hand side of the FLC cannot be determined by this procedure. The short free length of the specimen and the high stiffness of the testing machine enabled stable test performance and thereby recording of the complete stress-strain curve, including the softening branch. The test procedure can therefore be used for development and verification of fracture mechanics models.

Chen and Lin (2007) [50] investigated the effects of process parameters on the formability of deep drawing of rectangular cups of SUS304 stainless steel using both the simulations and the experiments. The material properties, the shape of the blank, die corner radius, punch radius etc. affect the material flow rate. Stress-strain curve was determined by performing the tensile tests on the specimens made of 0.61mm thick sheet which was cut along planes coinciding with the rolling directions of (0°), 45° and 90° and the FLD was determined using sheet specimens with widths ranging from 20mm to 140mm with an increments of 20mm by conducting hemi-spherical punch draw tests for SUS304 stainless steel. In the location closest to the fracture for each specimen, the major strain and minor strain were recorded. For the prediction of fracture in the finite element analysis, the design curve was used as the failure criterion. The process parameters are identified like punch radius, die radius, die corner radius, clearance and the length to width ratio.

Rodrigues *et al.* (2007) [51] compared the formability behaviour of friction stir welded aluminium blanks with wide weld beads and Laser steel welded blanks with narrow weld beads. A tailor-welded blank of 1mm thick is prepared by considering similar and dissimilar conditions of the two steel alloys (DC06 and DP600) and two aluminium alloys (AA 5182-H111 and AA 6016-T4) Steel. Circular specimens with 200mm diameter were extracted from the parent material sheets from TWBs to perform formability tests. By using a specially developed Deep-Drawing laboratorial testing device to work in a classical tensile test machine, the formability behaviour of the TWBs was analysed. The hardness between the welds and the base materials, for both similar welds, induced very small changes in mechanical properties in weld area in this case. For the dissimilar weld it is possible to expect a relatively good homogeneity in macroscopic mechanical properties for both similar and dissimilar aluminium TWBs. The formability tests of the AA 5182-H111 and AA 6016-T4 base materials and its similar welds show that they suffer strong wrinkling associated with severe changes in microstructure of the material, thickness of the weld relative to the base material, which induces non-homogenous behaviour of the blank and surface finishing.

Jose (2009) [52] examined the formability curves of AZ31 magnesium alloy sheet under the influence of forming process temperature, using the strain gradient evolution model predicting the forming limit curve from material plastic properties and initial thickness imperfections. The conclusions drawn by comparing the theoretical strain gradient with the experimental results of FLC of AZ31 magnesium alloy sheet deformed at high temperatures were:

1. By adopting a normalized strain gradient equal to 9, the above correlation was reasonably good.
2. At the beginning of diffuse necking or at the uniform deformation stage in the sheet metal forming, the strain gradient for the inception of local necking was predicted.
3. The work hardening coefficient, n-value and the strain rate sensitivity, M-value influence the FLC.
4. At high temperatures, the formability of AZ31 Mg alloy can be characterized by the measurement of M-value.

Reza *et al.* (2012) [53] studied the effects of punch and die temperature on the formability of a cup shaped AA3003 aluminium alloy sheet. The formability improves as the temperature difference between the punch and the die increases. Also the forming speed does not affect localized necking for the given punch velocities in the study. The simulations were captured for both punch force and failure location. The important parameters to control the thickness reduction in the blank were identified as friction and blank holder force. The finite element analysis model was validated with the selected experimental cases.

## 2.5 Research gap

Stretch formability of sheet metals depends on temperature of sheets. Increase in sheet metals temperature increase the stretch formability, but ductility of sheet metals were observed at elevated sheet temperature from the existing literature. To overcome the excessive ductility of sheet metal, annealing in between elevated temperature and room temperature was needed.

# CHAPTER 3

## MATERIAL AND METHODOLOGIES

### 3.1 Materials

The Material selected for this study was AA6023-T6 alloy sheet which have 2 mm thickness. AA6023-T6 alloy sheet has many application area in modern manufacturing industries. The products manufactured from the sheet metal by stretch forming process depend on the type of materials used. AA6023-T6 alloy has good mechanical properties and light weight that increase the application in automotive, aerospace, and aircraft compared to other metals.

### 3.2 Methodologies

Many different theories were formulated for analysis of stretch forming process and there were many approaches existed for analysis of the material behaviour of the deformation process. For this study some of sheet metal forming analysis approaches were used to evaluate the mechanical property of AA6023-T6 alloy sheet with experimental and theoretical. The general following diagram for evaluation of stretch formability of AA6023-T6 alloy sheet is indicated in Fig 3.1.

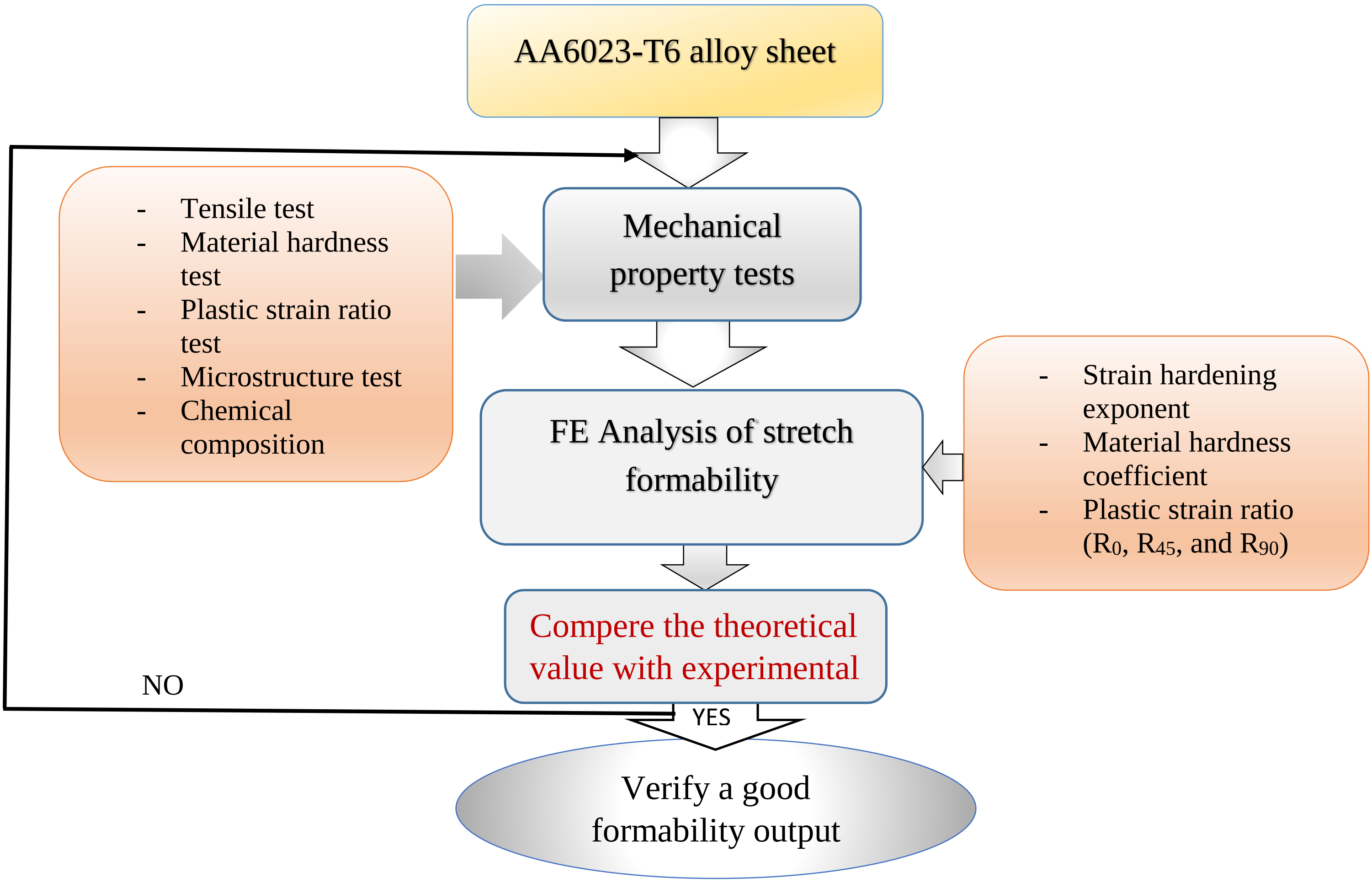


*Figure 3.1 General follow diagram of stretch formability evaluation*

## 3.3 Heat treatment process

Heat treatment is heating and cooling operations used to bring about a desired change in the physical properties of the materials. Its purpose is improve the structural and physical properties for some particular use or for future work of the metal. There are five basic heat treating processes: hardening, case hardening, annealing, normalizing, and tempering. For this study the annealing process was selected. Although each of the processes bring about different result in the metal, all of them involve three basic steps: heating, soaking and cooling [4].

### 3.3.1 Annealing process

AA6023-T6 alloy sheet was annealed to relieve its internal stresses, soften, made ductile and refine its grain structure. AA6023-T6 alloy sheet was annealed by heating to the temperature of 400$^{o}$C, and held at 400$^{o}$C temperature for 90 minutes and cooled back to room temperature. The cooling process for annealing done by burying the hot par in sand, ashes, or some other substance that does not conduct heat. Cooling process of AA6023 alloy sheet specimens was done by furnace cooling.

### 3.3.2 Heating process

Many alloys change structure when they were heated to specific temperature. For this study AA6023-T6 alloy sheet was heated at 400$^{0}$C to observe change in mechanical properties.

### 3.3.3 Soaking process

Once AA6023 alloy parts heated to the temperature of 400$^{o}$C at which changes in structure takes place, it must remained at that temperature until the entire part evenly heated called soaking process. The soaking time used for this work is 90 minutes.

### 3.3.4 Cooling process

After AA6023 alloy parts properly soaked, the third step is cool process. Here again, the structure may change from one chemical composition to another, it may stay the same, or it may revert its original form. An alloy after heating may stay the same during cooling deepening on the type of alloy and the rate of cooling. For this study the furnace cooling process was done.

## 3.4 Microstructure and hardiness tests

Microstructure of AA6023-T6 alloy sheet were studied by optical microscope. Optical microscope (model Huvitz HR-300 series) was used for microstructure testing process. The samples tested was prepared in to smaller size and mounted on the polyester resin and polished with silicon carbide papers and oral suspension of diamond paste. Before microstructure test the polished sample were etched with Keller’s enchant. The procedures for specimen’s preparation of microstructure test:

a) Cutting of the specimens in to small pieces for mounting process

b) Mounting with polystyrene resin

c) Polishing the samples with different grit size of sand papers
d) Polishing the samples with silicon carbide paper with diamond suspension
e) Washing and drying the samples until the finest surface finish reached
f) Etching  samples in to Keller’s etchant
g) Conducting the test

### 3.4.1 Mounting process

The polystyrene resin powder was added to the opening of the mounting device shown in Fig 3.2 the samples was placed to the opening of device before adding of the resin powder. After adding of resin powder, the piston of the device lowered and the compression piston locked to avoid the opening of the piston. The powder and the samples of AA6023-T6 alloy sheet was mounted together inside of the device by exerted pressure and heat. After mounting the automatic cooling process was performed inside the device. Then after samples were ready to proceed the next process.

***Figure 3.2 Mounting press machine***

### 3.4.2 Polishing and etching process

AA6023-T6 alloy sheet samples were polished using high performance diamond suspension on rotating silicon carbide paper as shown in Fig 3.3. After proper polishing the samples were immersed in to Keller’s etchant shown it Table 3.1 for 15 seconds.


***Figure 3.3 Rotating silicon carbide paper with diamond suspension***

Table 3.1 Keller's etchant used for microstructure observation

| Keller's etchant | Concentration | Condition |
|---|---|---|
| Methanol | 25 ml | 15 seconds |
| Hydro-chloric acid | 25 ml | |
| Nitric acid | 25 ml | |
| Hydrofluoric acid | 1 drop | |

### 3.4.3 Hardness tests

Vickers hardness (VHR) test was conducted to check the difference between hardness of annealed sheet samples at $400^0$C and at room temperature. The Vickers hardness test used a square-based pyramid diamond indenter with an angle of $136^0$ between the opposite face at the vertex, which was pressed in to the surface of the test piece using 10 kg and 5 kg forces. There was five trials performed for each samples and the average hardness (HV) was taken.

## 3.5 Uniaxial tensile test

Uniaxial tensile test was used to determine the reaction of AA6023 alloy sheet metal at room temperature and after annealing at temperature of 400$^{o}$C with 90 minute soaking time. In tensile test, sample was typically pulled to its breaking point to determine the ultimate tensile strength of the sheet. The amount of load applied to the specimen and the elongation of the specimen were measured throughout the testing process. The properties of a materials were expressed in terms of stress, which is the ratio of applied force to the area and strain, which was the percent change in length. To obtain the result of stress during the test, the force measurements were divided by the sample's cross-section area as shown in equation 3.1 and the value of strain is also obtained from equation 3.2 [4], by dividing change in length to the original length of the specimen. Both the value of stress and strain presented on X-Y plot or stress-strain curve.

$$\sigma = \frac{F}{A} \quad \ldots\ldots\ldots\ldots\ldots\ldots\ldots\ldots 3.1$$

$$\varepsilon = \frac{\Delta L}{L} \quad \ldots\ldots\ldots\ldots\ldots\ldots\ldots\ldots 3.2$$

### 3.5.1 Sample preparation

The standard specimen used for uniaxial tensile test was shown in Fig 3.4 and the ASTM E 8 M – 638 standard dimensions were listed in Table 3.2. The specimens are prepared by cutting three different orientation from 2mm thick aluminium alloy with AA6023 series sheet in the orientation of rolling direction ($0^{0}$), transvers direction ($90^{0}$) and diagonal direction ($45^{0}$).


*Figure 3.4 Typical specimen for tensile tests*

Table 3.2 ASTM E 8 M – 638 Standard dimensions of tensile test specimen [54]

| Dimensions | mm |
|---|---|
| Gauge length, G | 50 +/- 0.1 |
| Width, w | 12.5+/-0.25 |
| Thickness, T | 2 |
| Radius, R | 12.5 |
| Length of cross-section, A | 75 |
| Length of grip section, B | 50 |
| Width of grip section, C | 25 |

### 3.5.2 Experimental setup

The specimen for uniaxial tensile test was held by top and bottom griper attached to ISO 68982-1 universal testing machine shown in the Fig 3.5. The piston speed of the machine was automatically adjusted with the dimensions of the specimens. During the tension test, the grips were moved a part at constant rate to pull and stretch the specimen. The force on the specimen and its displacement was continuously monitored and plotted on a stress strain curve until fracture. The measurements, tensile strength, yield strength, and ductility were calculated after the tensile test specimen broken. The test specimen put back together to measure the final length, then this measurement was compared to the original length of the specimen. The same manner to final cross-sectional area of the sample compared to the initial cross-sectional area.


*Figure 3.5 ISO 68982-1 Uniaxial tensile testing machine*

### 3.5.3 Stress-strain relationship

During tensile test, the dimensions of the specimen changes with the deformation process, hence true quantity are better indicator of the engineering quantities. The engineering quantities of strain and stress are depend on the original dimensions of the sample. From tensile test, the value of the progress of load and change in length per time was used to calculate the engineering strain and stress. The original length, 'L' is taken from original gauge length from the standard sample.

Engineering strain, $e = \frac{\Delta L}{L}$ ……………………………………………3.3

Engineering stress, $S = \frac{F}{A}$ …………………………………………...3.4

The value of true strain and true stress are not depends on the original dimensions of the samples.

True strain, $\varepsilon = ln\ (1+e)$ …………..…………………………….……….3.5

True stress, $\sigma = S^*\ (1+e)$ ……………………………………………......3.6

### 3.5.4 Strain hardening

When a ductile material undergo the plastic deformation, the strength of the material increase. This phenomenon is called the strain hardening. Hollomon equation describes the strain hardening behaviour of sheet metal deformation. The Hollomon's equation was given by:

$$\sigma = K\varepsilon^{n}$$ ………………………………….……….3.7[4]

where, '$\sigma$' is true stress, for particular true strain '$\varepsilon$', 'k' is the materials strength coefficient, and 'n' is the material work hardening coefficient. The strain hardening exponent 'n' is used to measure the amount of strain hardening. It is a constant value calculated from the slope of natural logarithmic value of true strain-true stress graph. The natural logarithmic value of true strain and true stress was selected from the value in between yield strength and ultimate tensile strength. To plot the graph between $ln\ (\sigma)$ and $ln\ \varepsilon$, the equation, $ln(\sigma) = ln(k) + n ln(\varepsilon)$, used in the same way of the equation of line: $Y = C + mX$

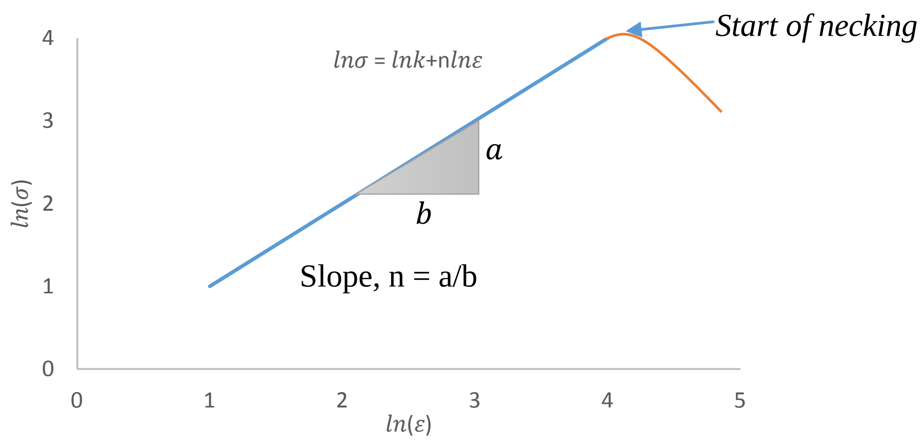


*Figure 3.6 Schematic graph of Natural logarithmic of true stress-train*

The formability of the sheet metal depends on the stain hardening coefficient value. A metal with larger value of strain hardening coefficient 'n' value has good formability than a materials with low value of strain hardening coefficient, because, the metal with highest value of strain hardening coefficient 'n' resist the increase in necking and it allows stretching farther before necking starts. Increasing the ability of metal to be elongated before necking increase the formability of the sheet metal.

### 3.5.5 Hill 1948 yield criterion

Rodney Hill in 1948 proposed an anisotropic yield criterion which was an extension of Von- Mises criterion. The anisotropy is termed as the directionality of the properties and it is associated with the variance of ionic spacing with in the crystallographic direction. For example, the crystal grains were oriented in the deformation specific directions making the- materials anisotropic in the case of permanent plastic deformation. Many anisotropic materials are validated using the Hill's Yield criteria. The general Von Mises yield criterion for isotropic material is expressed as:

$$(\sigma_{11} - \sigma_{12})^2 + (\sigma_{22} - \sigma_{33})^2 + (\sigma_{33} - \sigma_{11})^2 + 6(\sigma_{12}^2 + \sigma_{23}^2 + \sigma_{31}^2) = 6k^2 \ldots\ldots\ldots\ldots\ldots\ldots 3.8$$

This criterion has validated the plastic potential of many common materials which undergo uniform deformation in all directions. The Hills Yield criterion used to determine the initial yield surface and the equivalent plastic strain. In his equation, Hill considers tensile stress and compressive stress at the same yield stress and the homogenous quadratic with no single shear stress occurs linearly. Also there is no hydrostatic pressure effect on yielding. Hence, the plastic potential assuming the orthogonal principle axes as reference takes the form:

$$2f = + F(\sigma_{22} - \sigma_{33})^2 + G(\sigma_{33} - \sigma_{11})^2 + H(\sigma_{11} - \sigma_{12})^2 + 2L\sigma_{23} + 3M\sigma_{31}^2 + 2N\sigma_{12}^2 \ldots\ldots 3.9$$

At this condition the anisotropy of the material is given from the constants F, G, H, L, M, and N of equation 3.11. The normal yield stress determined experimentally are:

$$F = \frac{(\sigma^0)^2}{2}\left[\frac{1}{(\sigma^y{}_{22})^2} + \frac{1}{(\sigma^y{}_{33})^2} - \frac{1}{(\sigma^y{}_{11})^2}\right] \ldots\ldots\ldots\ldots\ldots\ldots 3.10$$

$$F = \frac{(\sigma^0)^2}{2}\left[\frac{1}{(\sigma^y{}_{33})^2} + \frac{1}{(\sigma^y{}_{11})^2} - \frac{1}{(\sigma^y{}_{22})^2}\right] \ldots\ldots\ldots\ldots\ldots\ldots 3.11$$

$$F = \frac{(\sigma^0)^2}{2}\left[\frac{1}{(\sigma^y{}_{11})^2} + \frac{1}{(\sigma^y{}_{22})^2} - \frac{1}{(\sigma^y{}_{33})^2}\right] \ldots\ldots\ldots\ldots\ldots\ldots 3.12$$

The shear stresses are:

$$L = \frac{3(\tau^0)^2}{2(\tau^y{}_{23})^2} \ldots\ldots\ldots\ldots\ldots\ldots\ldots\ldots\ldots\ldots 3.13$$

$$M = \frac{3(\tau^0)^2}{2(\tau^y{}_{31})^2} \ldots\ldots\ldots\ldots\ldots\ldots\ldots\ldots\ldots\ldots 3.14$$

$$N = \frac{3(\tau^0)^2}{2(\tau^y{}_{12})^2} \ldots\ldots\ldots\ldots\ldots\ldots\ldots\ldots\ldots\ldots 3.15$$

Where, $\sigma^0$ and $\tau^0$ are the reference stresses. The equivalent stress for the yield criterion is given by:

$\bar{\sigma} = \sqrt{F(\sigma_{22} - \sigma_{33})^2 + G(\sigma_{33} - \sigma_{11})^2 + H(\sigma_{11} - \sigma_{22})^2 + 2L(\sigma_{23})^2 + 3M(\sigma_{31})^2 + 2N(\sigma_{12})^2}$…
………………3.16 [4]

## 3.6 Plastic strain ratio

When a sheet metal is subjected to either tensile or compressive load, thinning or thickening occur, this thinning or thickening is opposed by the sheet metal during load application. The parameter that shows the ability of sheet metal to resist the thinning or thickening is the value of (r) or plastic strain ratio. Within the polycrystalline metal the plastic strain ratio is related to selected crystallographic orientation and it is a plastic anisotropy measure. The formability of sheet metal depend upon the resistance of thinning or thickening. The shapes formed by deep-drawing process have cylindrical flat-bottom cups because of resistance of thinning or thickening of sheet metal. The plastic strain ratio is useful for evaluating materials selected for forming different shapes geometries. On uniaxial tensile test of plastic strain ratio, the specimen pulled between gripers to the length direction and change in gauge length and thickness is recorded. Analytically the plastic strain ratio ‘r’ is the ratio of true width strain to true thickness strain.

$$r = \frac{\varepsilon_w}{\varepsilon_t} \ldots\ldots\ldots\ldots\ldots\ldots\ldots 3.18$$

Where, $\boldsymbol{\varepsilon}_w$ and $\varepsilon_t$ are the strain in width and thickness direction respectively, and the vales of $\boldsymbol{\varepsilon}_w$ and $\varepsilon_t$ are calculated by using equation 3.19 and 3.20 respectively.

$$\varepsilon_w = ln\left(\frac{w_f}{w_o}\right) \ldots\ldots\ldots\ldots\ldots\ldots 3.19$$

$$\varepsilon_t = = ln\left(\frac{t_f}{t_o}\right) \ldots\ldots\ldots\ldots\ldots\ldots\ldots 3.20$$

Assuming that there is no change in volume or at constant volume during test, the plastic strain ratio calculated by the following formula.

$$r = \frac{ln\left(\frac{w_f}{w_o}\right)}{ln\left(\frac{L_o w_o}{L_f L_f}\right)} \ldots\ldots\ldots\ldots\ldots\ldots\ldots 3.21$$

The plastic strain ratio values was measured by digital calliper at 2% elongation and calculated by plastic strain ratio formula using in the equation 3.18 to equation 3.21.

### 3.6.1 Experimental setup

In tensile stress testing, the value of plastic strain ratio is associated with gradient of corresponding component strain plot. When the plot of strain is linear the value of plastic strain is constant, so that in the ratio, total plastic strains may replace incremental strain. The ASTM-E517 standard specimen used for the test of plastic strain ratio is shown in Fig 3.7. The dimensions of the specimens are listed in Table 3.3. The specimens are prepared by cutting three different orientation from 2mm thick aluminium alloy with AA6023 series sheet in the orientation of rolling direction ($0^0$), transvers direction ($90^0$) and diagonal direction ($45^0$). In plastic strain ratio test, the length and width of the specimen are not critical. But, special care was taken to stretch the gage section in uniform manner to avoid griper effects and anomalous change along gauge length.

***Figure 3.7 ASTM-E517 standard specimens for plastic strain ratio test***

Table 3.3 ASTM-E517 Standard dimensions of specimens for plastic strain ratio test [54]

| Dimensions | mm |
|---|---|
| Gauge length, G | 50 +/- 0.1 |
| Width, w | 12.5+/-0.25 |
| Thickness, T | 2 |
| Radius, R | 12.5 |
| Length of cross-section, A | 75 |
| Length of grip section, B | 50 |
| Width of grip section, C | 25 |

The experimental set up for the test of plastic strain ratio is shown in Figure 3.8.


***Figure 3.8 Experimental set up for plastic strain ratio test***

### 3.6.2 Procedure of experiment

1. The original width of the specimen, $w_o$ is marked to dimension of 2 millimetre at the mid-point of the specimen.
2. The original length of the specimen, $l_o$ is marked to dimension of 2 millimetre at the mid-point of the specimen
3. The specimen pulled axially until 2% elongation, then the process was stopped.
4. The final width $w_f$, and gauge length $l_f$, is measured in similar manner to initial measurements.

## 3.7 Simulation details

Finite element method was used for numerical analysis of sheet metal forming operations. The numerical analysis of stretch forming process was done by PAM STAMP 2G software. The input model consists of die, blank, blank holder, draw and punch  have been constructed in pre-processor. The punch, die and blank holder has been considered as rigid body. The fine meshing has been done on the surface of die, blank holder and punch, since, the blank has been considered as a deformable body. The assembly of LDH setup in PAM STAMP 2G is shown in Fig 3.9.

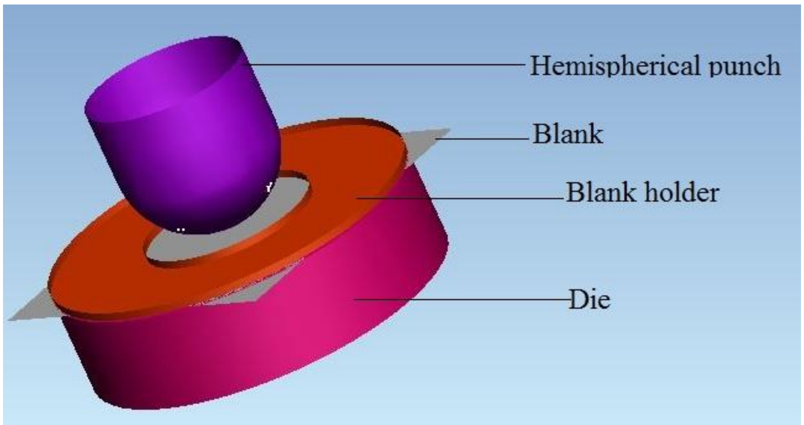


***Figure 3.9 Assembly of LDH setup in PAM STAMP 2G with blanks***

In a LDH test, the blank with 2mm thickness is deformed by a hemispherical punch (diameter: 101.6 mm) inside opening of a die with 105.9 mm diameter. For simulations process, five tests with different size of blanks were used for each ($0^0$), ($45^0$) and ($90^0$) orientation of samples. Fig 3.10 indicates the dimensions of each blanks used for LDH tests. The tools required for LDH test, punch, die, blank holder, draw bead, and blank generated in solid works, a CAD packages, and meshed using delta mesh facility in PAM STAMP 2G. Both Hollomon's strain hardening law and Hill's 1948 isotropic hardening yield criterion were used as the plasticity model. The coefficient of friction $\mu$ in the process used to alter the amount of-lubrication during deformations. The blank was as the active body and the punch force used was 80 KNs  to avoid the drawing and tearing near draw beads during forming prediction.

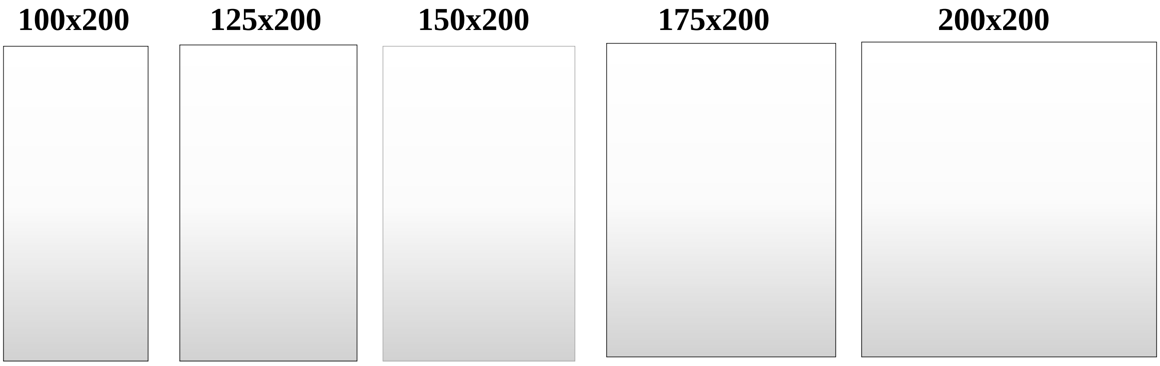


***Figure 3.10 Schematic representation of blanks and their dimensions for LDH tests***

### 3.7.1 Forming parameters for LDH tests

The main forming parameters used were the coefficient of friction $\mu$, punching force, and forming speed. The assumptions of parameters are listed in the Table 3.4.

**Table 3.4 Forming parameters for LDH tests**

| Parameters | values |
|---|---|
| Hemispherical punch radius | 101.6 mm |
| Die profile radius | 105.9 mm |
| Blank material | AA6023 – T6 |
| Blank thickness | 2 mm |
| Punching force | 80 KN |
| Blank holder force | 80 KN |
| Forming speed | 10 mm/s |
| Coefficient of friction | 0.2 |
| Element type | 4 node rectangular |

### 3.7.2 Thickness gradient based necking criterion

A thickness gradient based necking criterion was used to obtain the displacement at the failure of the blanks. This thickness based necking criterion was found from the experiment that necking occurs in the sheet metal when the thickness gradient or the ratio of thickness of neighbouring element falls below 0.92 [50]. Hence, in the present simulations the necking elements were considered as the element pair where the thickness ratio equals or below 0.92. Necking can be understood as a thinning phenomenon and it basically perceives necking as localized thinning phenomenon. A localized thinning region within deforming sheet, where a steep gradient in thickness develops. A local critical thickness gradient ($Rc$) must exist at the onset of a local visible neck. In the simulations, the thickness gradient developed in the adjoining element of size 2-5 mm was mentioned, when this gradient ($R_{\text{actual}}$) drops below a critical values, it is calculated that the local necking has initiated in the element where thickness is lowered. When the necking criterion satisfied the maximum load and displacement at failure were noted. A similar procedures was followed for all samples in longitudinal, transvers and 45 degree oriented during LDH tests. Thickness gradient based criterion is related to the physical necking phenomenon and hence can be associated with FE simulations directly. This limit strain criterion is sensitive to the meshing size of the element. From the previous studies it was found that the meshing size should be (1 – 5 mm) to follow this necking failure criterion. Mesh size for FE simulation used in this study was (2 mm) to overcome the sensitivity of the limit strain criterion. The schematic illustration of the applicability of this criterion is shown in Fig 3.11 [55].

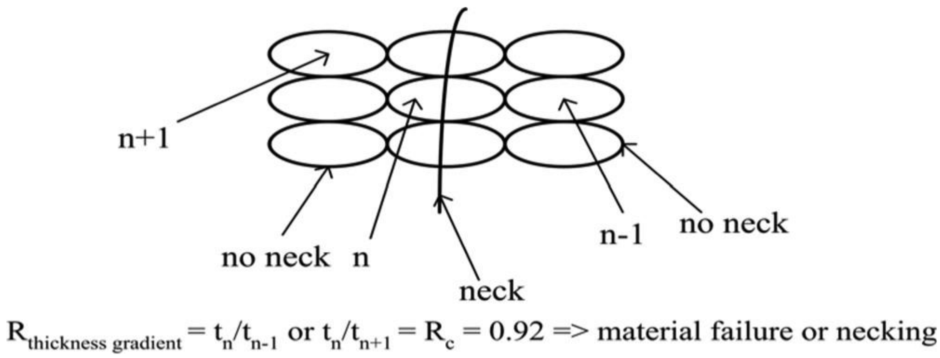


***Figure 3.11 Schematic illustration of thickness gradient – based necking criterion*** **[55]**

# CHAPTER 4

## RESULTS AND DISCUSSION

### 4.1 Chemical composition

**Table 4.1 Chemical composition of AA6023-T6 alloy sheet**

| Chemical composition | | | | | | | | |
|---|---|---|---|---|---|---|---|---|
| Si | Fe | Cu | Mn | Mg | Bi | Sn | Residuals | Al |
| 0.57% | 0.5% | 0.19% | 0.24% | 0.41% | 0.3% | 1.2% | 0.59% | 96% |

The chemical composition of AA6023-T6 alloy sheet used in this study was found form x-ray test shown in the Table 4.1.

### 4.2 Tensile properties

Mechanical properties of AA6023-T6 alloy sheet are obtained from uniaxial tensile test. Figure 4.1 and 4.2 shows the uniaxial tensile test samples before fracture and after fracture respectively.

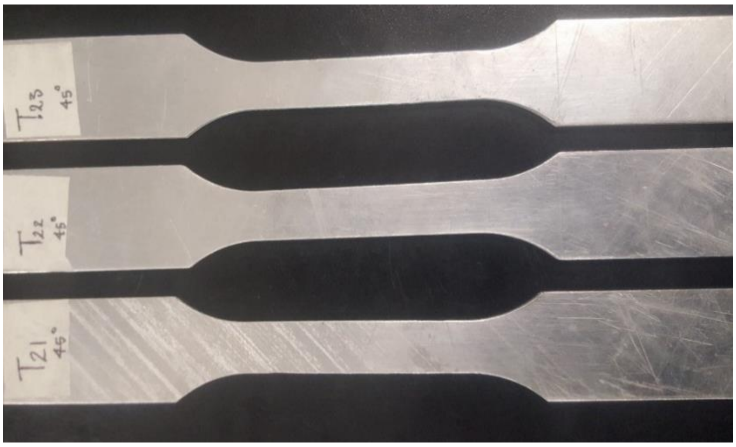

*Figure 4.1 Uniaxial tensile test samples before fracture*

From uniaxial tensile tests, the mechanical properties are evaluated and discussed in the followed topics including the simulation results of the LDH of the sheets. Figure 4.2 shown blow indicates the fracture behaviour of the sheet metal at different directions. For the rolling direction (RD) there is inclined fracture at some angle. For $45^0$ orientation there is parallel fracture with respect to the orientation. And for transvers (TD), perpendicular fracture to the rolling direction. In general there is some necking observed in all case of the samples.

***Figure 4.2 Uniaxial tensile test samples after fracture***

Table 4.2 gives the property of AA6023-T6 alloy sheet used for simulation of stretch formability. The mechanical properties and anisotropy value shown in Table 4.2 are the average experimental values obtained from tensile test and plastic strain ratio test. The material used has 2mm thickness and density, ρ($2.8x10^{-6}$ kg/$m^3$), poison's ratio, γ(0.33), and young modules E(68 Gpa) values are taken from aluminium alloy standard values.

**Table 4.2 Mechanical property of AA6023-T6 alloy sheet at room temperature**

| Orientation of samples | UE (mm) | UTS (MPa) | $\sigma_{ys}$ (MPa) | K (MPa) | n | $R_0$ | $R_{45}$ | $R_{90}$ |
|---|---|---|---|---|---|---|---|---|
| $0^0$ | 0.38 | 200 ±9 | 180±3 | 313±40 | 0.132 | 0.49 | 0.68 | 0.56 |
| $45^0$ | 0.54 | 208 ±4 | 190±18 | 338±20 | 0.134 | | | |
| $90^0$ | 0.52 | 212±12 | 200±12 | 358±20 | 0.133 | | | |

Heat treatment of the aluminium alloys causes change in mechanical and anisotropy values. Table 4.3 indicates the value of mechanical properties and plastic anisotropy of AA6023-T6 alloy sheet after annealing at $400^0$C with one and half hours soaking time.

**Table 4.3 Mechanical property of AA6023-T6 alloy sheet after heat treatment**

| Orientation of samples | UE (mm) | UTS (MPa) | $\sigma_{ys}$ (MPa) | K (MPa) | n | $R_0$ | $R_{45}$ | $R_{90}$ |
|---|---|---|---|---|---|---|---|---|
| $0^0$ | 0.19 | 206±13 | 170±17 | 326±33 | 0.149 | 0.43 | 0.58 | 0.47 |
| $45^0$ | 0.21 | 197±2 | 168±5 | 323±16 | 0.162 | | | |
| $90^0$ | 0.25 | 193±6 | 166±7 | 315±28 | 0.155 | | | |

## 4.3 Evaluation of microstructure

The result of microstructure tests indicating the difference between the AA6023-T6 alloy sheet at room temperature and annealed sheet at 400$^0$C. Figure 4.3 show the microstructure of sheets at room temperature and annealed sheet at 400$^0$C.

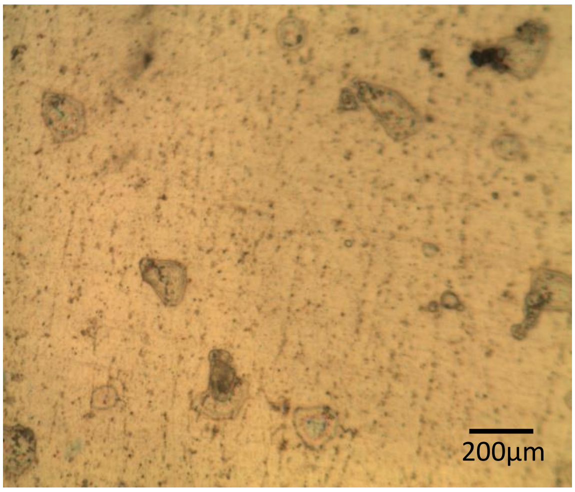


(a)

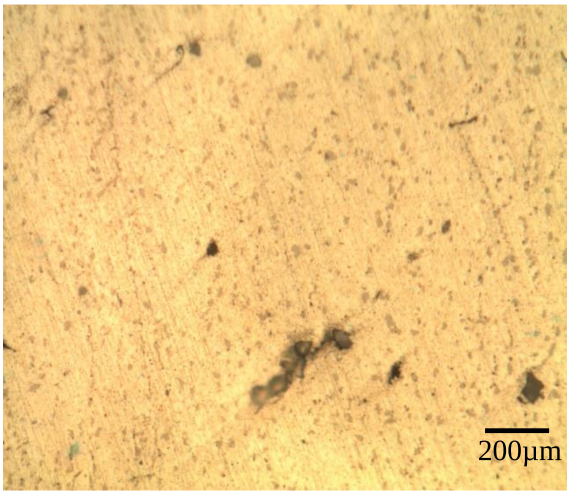


(b)

***Figure 4.3 Polished surface of AA6023-T6 samples: (a) before etching process and (b) after etching process***

Polished surface shown in Fig 4.3 (a) show the effect of annealing on the sample of alloy sheet. There is refined microstructure of sample as well as good surface compared to room temperature sample.

## 4.4 Evaluation of hardness

Observation form Vickers hardness (VHR) test, there is change in hardness of alloy sheets at room temperature and after annealing at 400$^0$C. For each samples five trials was performed with varying 5 kg and 10 kg load. Figure 4.4 indicate the surface of sample which hardness test was performed. Also Tables 4.5 and 5.6 show the trials of test for annealed and at room temperature samples.

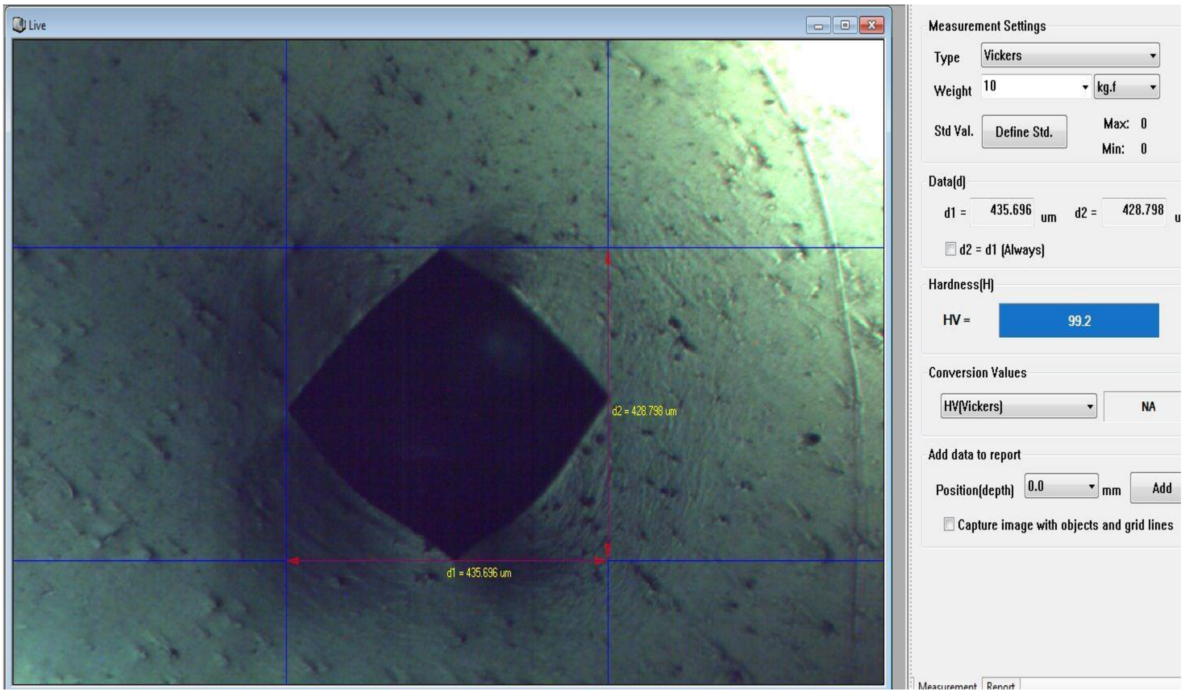


***Figure 4.4 Surface of hardness tested sample with 10 kg load***

**Table 4.4 Trails of hardness tests for room temperature sample**

| Hardness | | Trail - 1 | Trail - 2 | Trail - 3 | Trail - 4 | Trail – 5 | Average |
|---|---|---|---|---|---|---|---|
| HV | 5 kg | 51.5 | 50.6 | 51.7 | 52.8 | 50.6 | 51.44 |
| | 10 kg | 101.1 | 103 | 50.6 | 103.3 | 105.6 | 92.72 |

**Table 4.5 Trails of hardness tests for annealed sample**

| Hardness | | Trail - 1 | Trail - 2 | Trail - 3 | Trail - 4 | Trail - 5 | Average |
|---|---|---|---|---|---|---|---|
| HV | 5 kg | 49.6 | 24.2 | 25.2 | 25.2 | 49.6 | 34.72 |
| | 10 kg | 99.2 | 48.1 | 50.4 | 51.2 | 99.2 | 69.62 |

The difference between average hardness value (HV) of room temperature and annealed sample for 5 kg load is 16.72 and the difference between average HV of room temperature and annealed sample for 10 kg load is 23.1. Therefore, by taking the percentage average value of two different load conditions, the total reduction of hardness during annealing process is 0.2 %.

## 4.5 Evaluation of true stress-strain curves

The flow curve data obtained from nine tensile tests for normal (at room temperature) and nine tensile tests for heat treated (annealed), totally eighteen tensile tests for three different directions relative to rolling directions (RDs). Figures 4.5 and 4.6 show the true stress – true strain curves for annealed and normal samples respectively. The material's tensile data obtained from Fig 4.5 and 4.6 were used later in PAM STAMP 2G software for simulations.

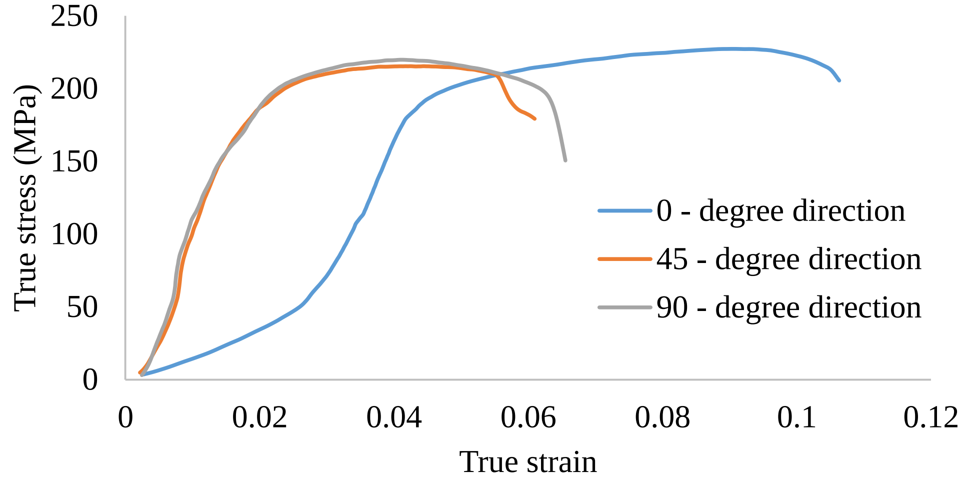


*Figure 4.5 True stress – true strain curve for samples at room temperature*

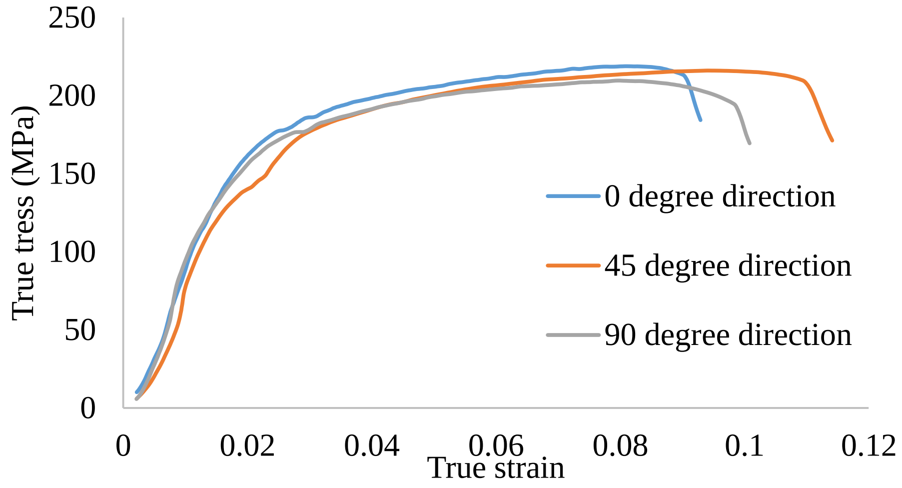


***Figure 4.6 True stress – true strain curve for annealed samples at 400$^0$C***

Figures 4.5 and 4.6 show the direct proportionality of the true stress with true strain. When stress value increased, true strain value are also increased. For a samples at room temperature, the increase in strain value is less for 45$^0$ direction samples and 90$^0$ (TD) samples compared to 0$^0$ longitudinal direction (LD) samples, which is less than true strain value of heat treated samples. For 45$^0$ and 90$^0$ oriented samples fracture occurs earlier than 0$^0$ (LD) sample at room temperature. The comparison between true stress – true strain curves on Fig 4.4 with true stress – true strain curves on Fig 4.5 indicates the increase in values of true strain for annealed samples. This relationship indicates the ductility of the sheet metal increased with annealing process. When the ductility of sheet metal increased, it obtain good formability.

## 4.6 Evaluation of stress concentration

Figure 4.7 show the major stress distribution of the blanks of $0^0$ oriented sheets at room temperature obtained from simulation of stretch forming test in PAM STAMP 2G. The stress distribution around surface and neck of the blank is indicated in red colour. The crack formation of the blank also takes place at these stress concentrated surfaces.

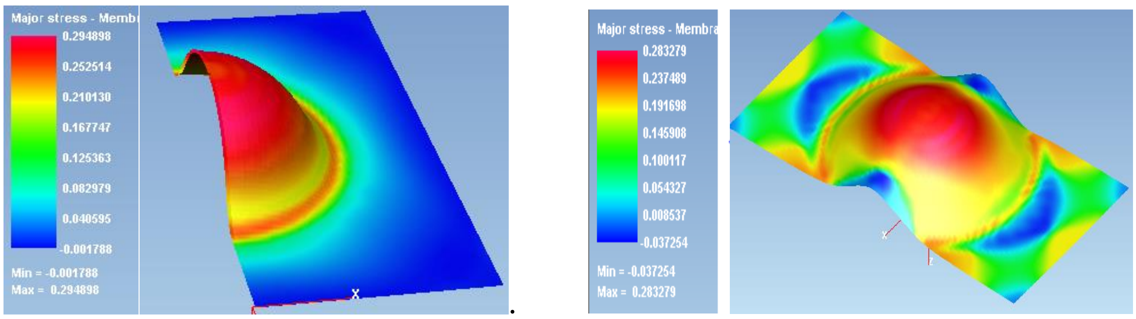


(a) (b)

***Figure 4.7 Major stress distribution of the blanks with $0^0$ orientations; (a) major stress concentration of 200x200 blank, (b) major stress concentration of 100x200 blank***

The major stress concentration showed in Fig 4.7 (a) and Fig 4.7 (b) above has significant effect on stretch formability. The maximum major stress for 200x200 blank in Fig 4.7 (a) is 0.29 MPa and its minimum value is 0.0018MPa. At this maximum major stress concentration the crack formation was started. The maximum LDH at maximum major stress concentration is 39 mm. The maximum major stress concentration for 100x200 blank in Fig 4.7 (b) is 0.28 MPa and its minimum value is -0.037MPa. The crack formation was started at this maximum major stress concentration. The maximum LDH at this stress concentration is 29 mm. The simulation result indicates, 200x200 blank has good stretch formability than 100x200 because, the maximum LDH was observe in 200x200 blank. But, maximum major stress concentration on 100x200 blank is less compared to 200x200 blank.

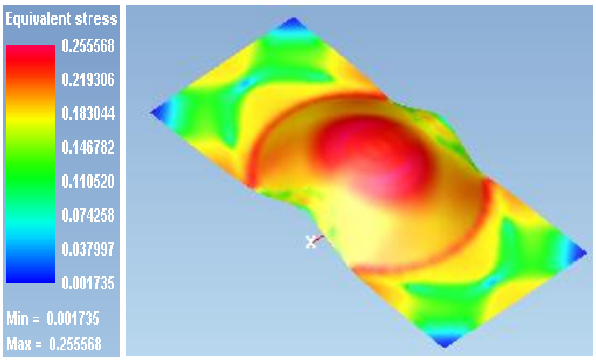


***Figure 4.8 Equivalent stress distribution of the blank with 100x200 $0^0$ orientation at room temperature***

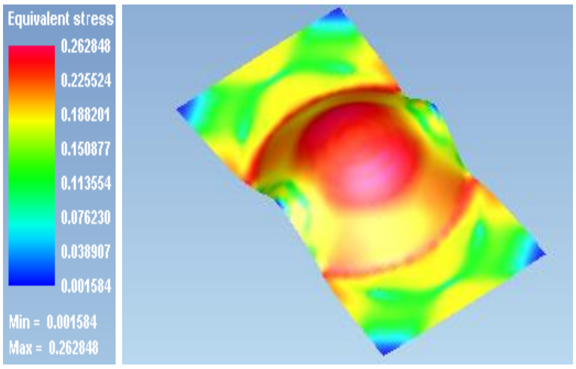


***Figure 4.9 Equivalent stress distribution of the blank with100x200 in $0^0$ orientation after annealing process***

Figures 4.8 and 4.9 show the equivalent stress concentration for sheets at room temperature and annealed at $400^0$C of $0^0$ orientation. The maximum equivalent stress for 100x200 blank at room temperature in Fig 4.5 is 0.26 MPa and its minimum value is 0.0017MPa. The maximum LDH at maximum equivalent stress concentration is 26 mm. The maximum equivalent stress for annealed 100x200 blank in Fig 4.9 is 0.26 MPa and its minimum value is 0.0016MPa. At this maximum major stress concentration the crack formation was started the same as in blank 100x200 in Fig 4.8. The maximum dome height at this stress concentration for annealed blank is 31mm. From the observation of LDH, annealed blank at $400^0$C shown in the Fig 4.9 has maximum LDH, which indicate it has good stretch formability than a blank at room temperature. Because, for a blank at room temperature condition crack formation is occurring earlier than annealed blank at $400^0$C.

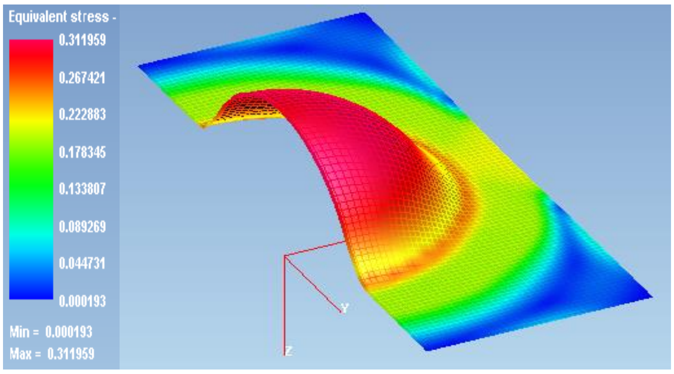


***Figure 4.10 Equivalent stress distribution of the blank with 150x200 in 45$^{0}$ orientation at room temperature***

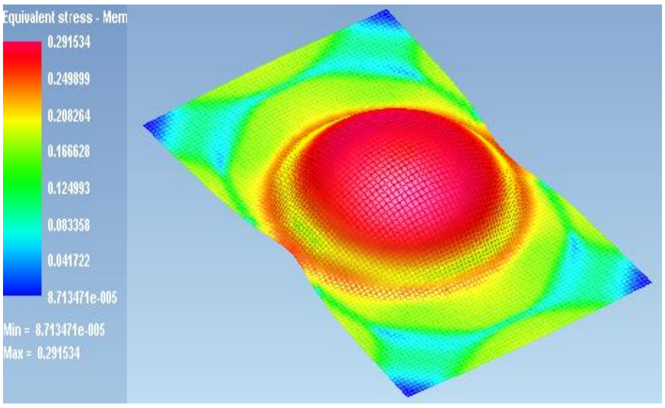


***Figure 4.11 Equivalent stress distribution of the blank with 125x200 in 45$^{0}$ orientation after annealing process***

Figure 4.10 show simulated value of the equivalent stress concentration for half sectioned view of 150x200 blank at room temperature in 45$^{0}$ orientation. The maximum equivalent stress concentration shown in red colour and it has 0.31MPa and minimum value is 0.00019MPa. At this maximum major stress concentration the crack formation was started due to local thinning. The maximum LDH at maximum equivalent stress concentration is 39 mm. The maximum equivalent stress for annealed 100x200 blank in Fig 4.11 is 0.29 MPa and its minimum value is 0.005MPa. The maximum LDH of annealed blank at maximum equivalent stress concentration is 42.5 mm. From LDH, annealed blank shown in the Fig 4.11 has maximum LDH which indicates, it has good stretch formability than blank at room temperature. Because, for blank at room temperature condition subjected to earlier crack formation than annealing blank condition even if the size of blank is smaller. Annealed blank at 400$^{0}$C has larger stress concentration than blank at room temperature, this is occurred due to the difference in size of blanks.

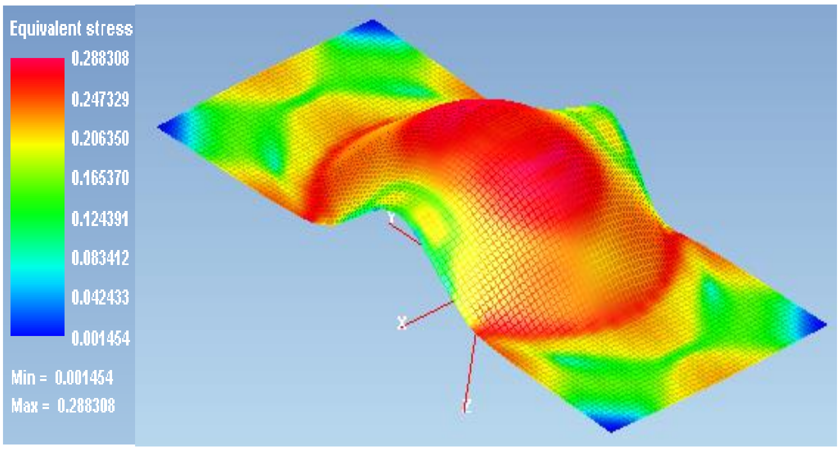


***Figure 4.12 Equivalent stress distribution of the blank with 100x200 in $90^0$ orientation at room temperature***

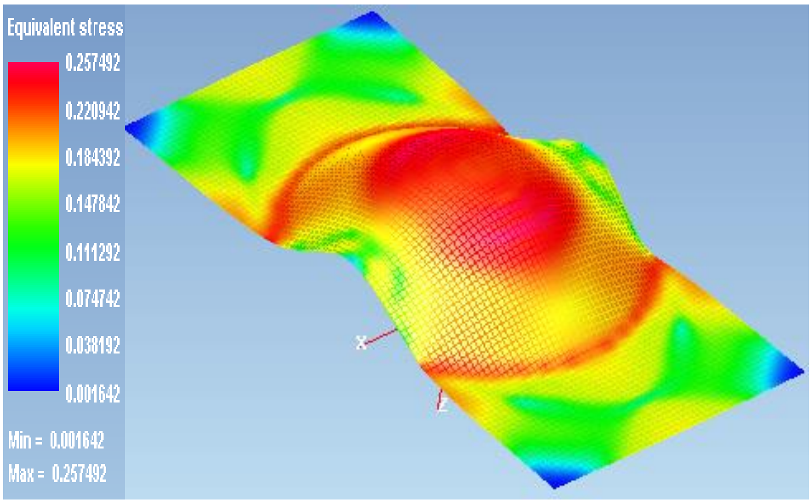


***Figure 4.13 Equivalent stress distribution of the blank with 100x200 in $90^0$ orientation after annealing process***

Figures 4.12 and 4.13 above show the equivalent stress concentration involved at the surface of deformation in blank at room temperature and annealing at $400^0$C of $90^0$ orientation. The maximum equivalent stress for 100x200 blank in Fig 4.12 is 0.29 MPa and its minimum value is 0.0015MPa. The maximum LDH at this stress concentration for blank at room temperature is 32 mm. The maximum equivalent stress for 100x200 blank in Fig 4.13 is 0.26 MPa and its minimum value is 0.0016MPa. At this maximum equivalent stress concentration the crack formation was started due to excessive thinning. The maximum LDH for annealed blank at $400^0$C is 30.5. Form LDH of the blanks, stretch formability difference is observed. Annealed blank at $400^0$C in the Fig 4.13 has minimum LDH which indicate the annealed blank has slightly less formability than blank at room temperature. In general, a good stretch formability was observed for annealed sheets at $400^0$C.

## 4.7 Evaluation of punch force versus displacement

The variation of punch force with displacement for annealed sheet at $400^0$C and sheets at room temperature were observed. The analysis was carried out by comparing the punch force and displacement of simulation results of heat treated sheets with sheets at room temperature.

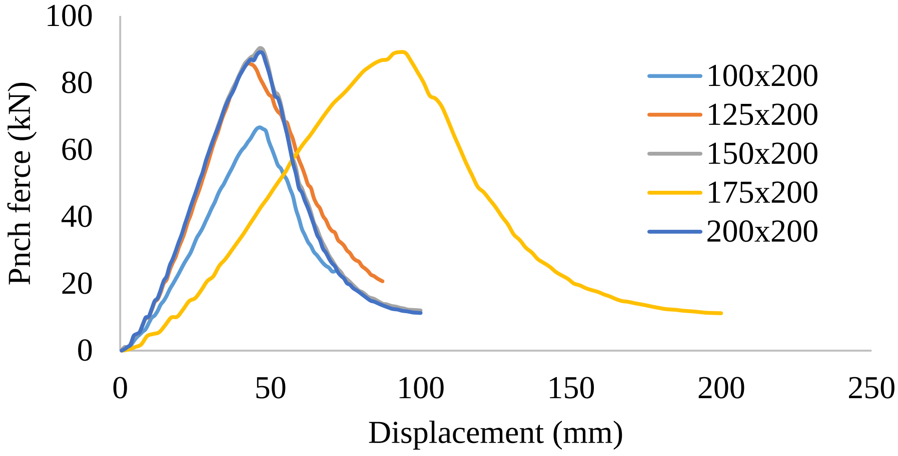


*Figure 4.14 Punch force with Displacement curves at room temperature of 0 degree direction*

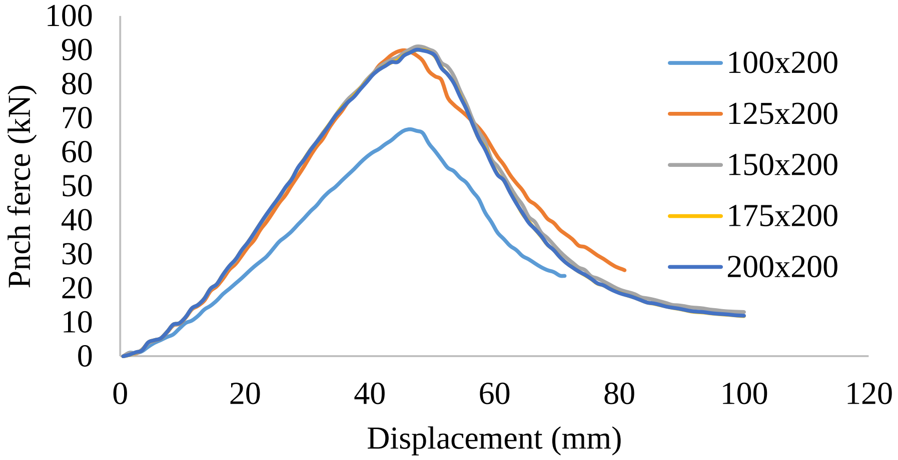


*Figure 4.15 Punch force with Displacement curves after annealing process of 0 degree direction*

Figure 4.14 above show punch force verses displacement curves at room temperature. In this Figure the punch force required for deformation of 100x200 blank before fracture is less than the punch force of the other four blanks. The blanks with dimensions of 150x200 and 200x200 lies at the same fracture punch force. A blank with dimensions of 125x200 requires slightly less punch force until fracture. The punch force has direct proportionality with the displacement of the blanks during deformation. With increase of punch force the displacement increase until the fracture, but after fracture the displacement increase with decrease of the punch force. Generally the maximum displacement value for room temperature sheets at $0^0$ oriented is less than 100mm except a blank with 175x200, it is in between 200mm. this displacement value of blank 175x200 reduced to 100mm by annealing process.

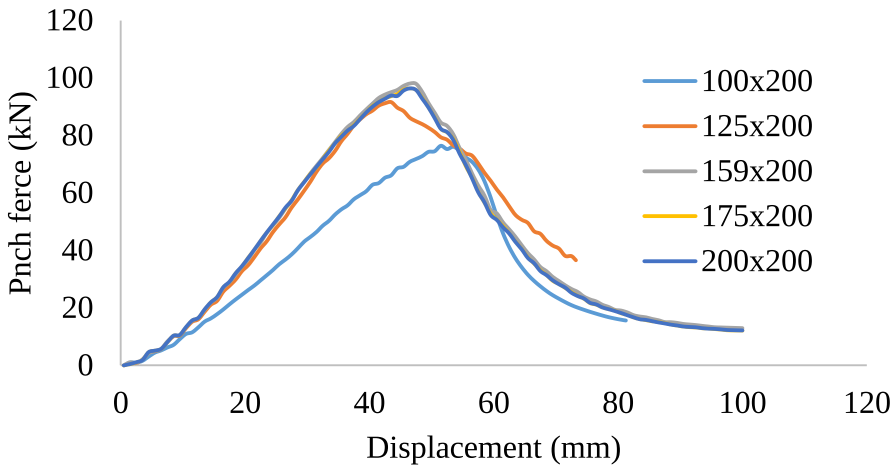


***Figure 4.16 Punch force with Displacement curves at room temperature of 45 degree direction***

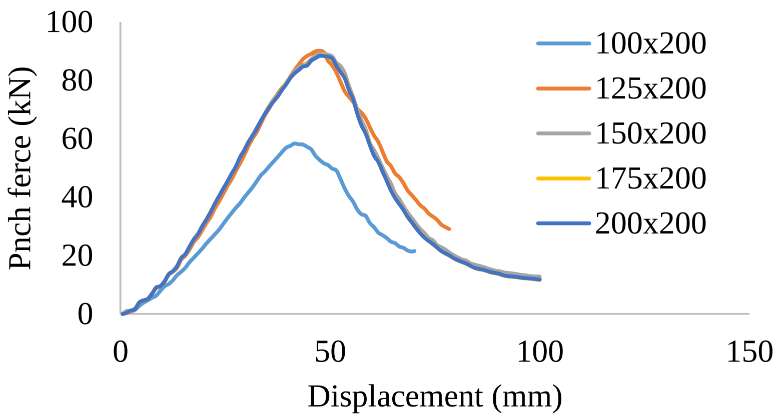


***Figure 4.17 Punch force with Displacement curves after annealing process of 45 degree direction***

Figures 4.16 and 4.17 above show punch force versus displacement curves at room temperature for $45^0$ direction samples. From Figures the difference between punch force need for annealed and normal samples are clearly observed. In general the punch force needed for corresponding displacement of the sheet is maximum (100 KN) to a samples non heat treated. For annealed samples the punch force required is 90 KN before fracture occurs. This indicates the deformation of the sheets at room temperature need much more punch force than annealed. In both case the punch force required to deform the sheet metal until fracture is minimum fore 100x200 size blanks compared to the other samples.

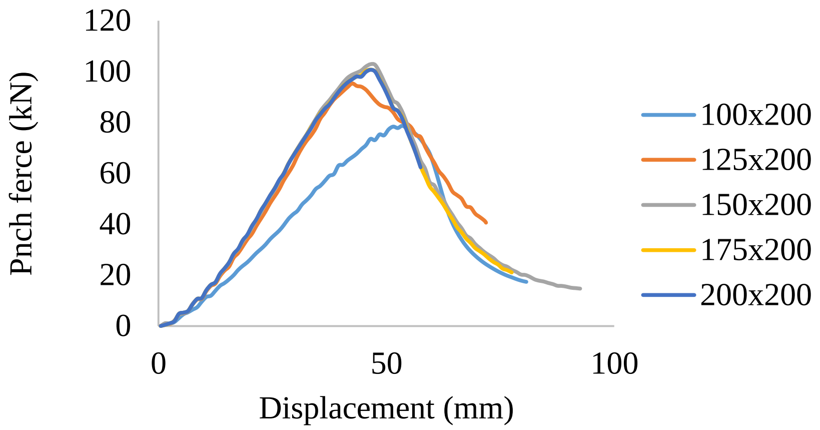


***Figure 4.18 Punch force with Displacement curves at room temperature of 90 degree direction***

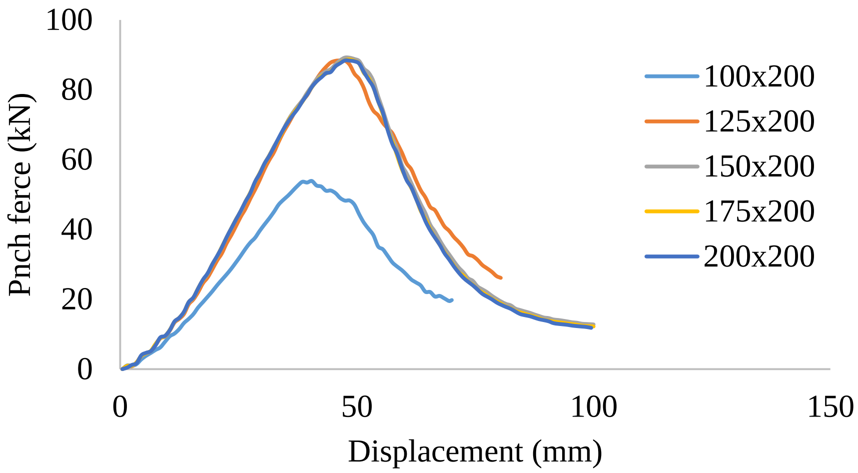


*Figure 4.19 Punch force with Displacement curves after annealing process of 90 degree direction*

From the above Fig 4.18 and 4.19 the relation between punch force with the displacement and annealing processes are observed. It is similar to $45^0$ direction sample, the punch force is minimum to 100x200 size blanks in both case, but in case of heat treated blank the displacement is minimum than non-heat treated blank. In general the punch force needed for corresponding displacement of the sheet is greater than 100 KN to a samples non heat treated and for annealed samples the punch force required is in between 80 and 100 KN before fracture occurs.

## 4.8 Evaluation of thickness distribution

Thickness distribution of the deformed blank is necessary criteria to chive a good formability of the sheet metal. The uniform thickness distribution of the blank has significant effect in formability. The thickness distribution of the different blanks are observed from one end of a sheet along the major strain direction and normal to the necking region. Fig 4.20 and 4.21 show the thickness distribution from one end of the sheet for different size of blanks at $0^0$ orientation sheets at room temperature and annealed sheets at $400^0$C respectively.

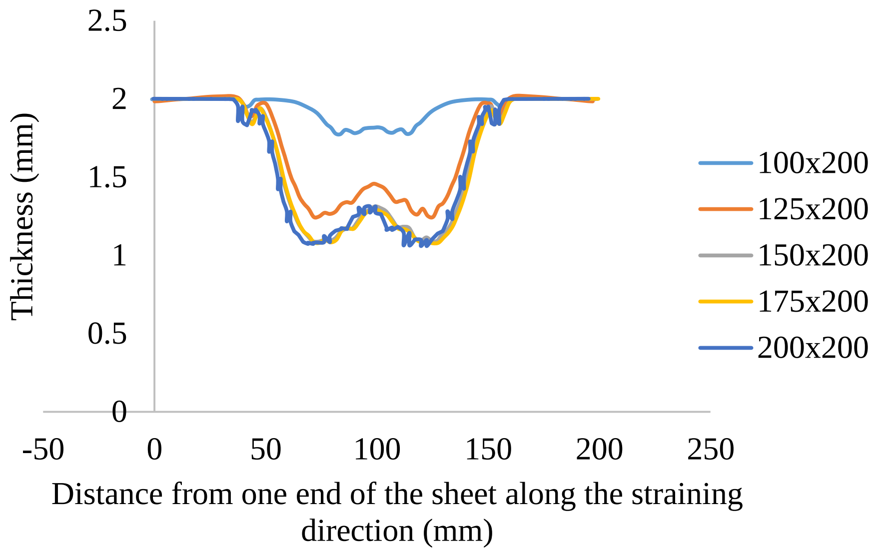


***Figure 4.20 Thickness distribution of $0^0$ oriented sheets at room temperature***

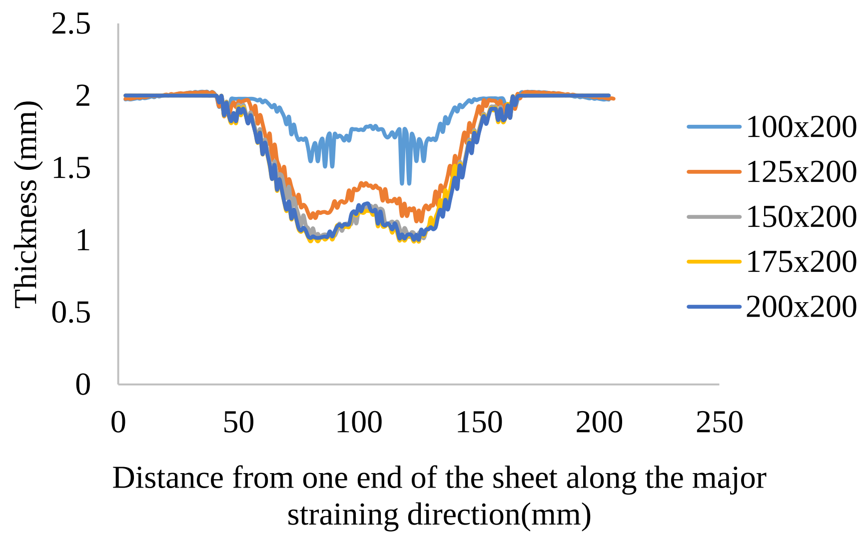


***Figure 4.21 Thickness distribution of $0^0$ oriented annealed sheets at $400^0$C***

Figure 4.21 show the thickness distribution along strain direction. Comparison of curves of sheets at room temperature in Fig 4.20 with curves of annealed sheets at 400$^0$C has uniform thickness distribution and the curve of blank 100x200 did not rich the maximum thickness distribution in curves of 150x200, 175x200 and 200x200 in both annealed and at room temperature. Curve of blank with 125x200 has grater thickness in both case compared to the other curves.

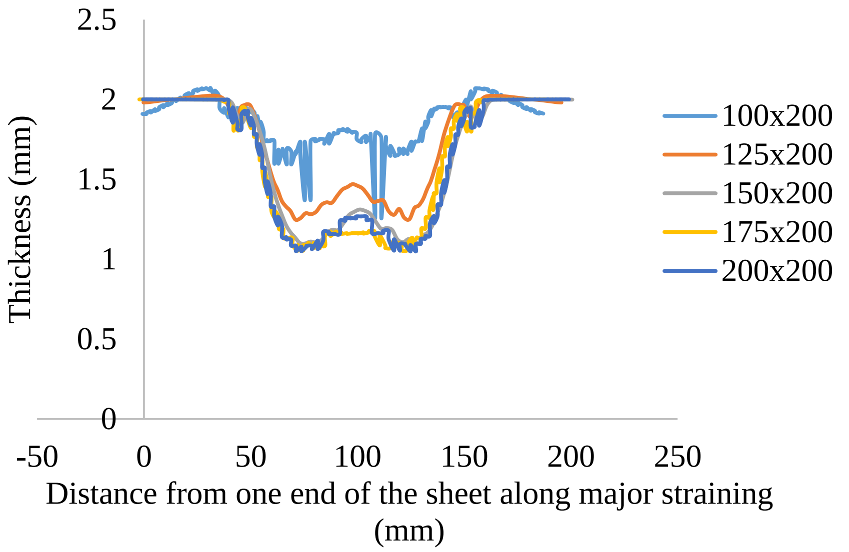


***Figure 4.22 Thickness distribution of 45$^0$ oriented sheets at room temperature***

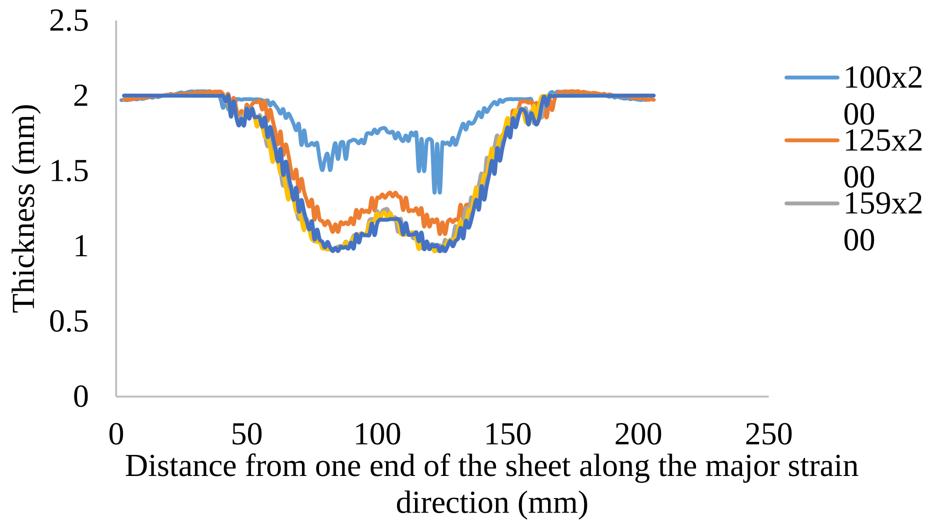


***Figure 4.23 Thickness distribution of 45$^0$ oriented annealed sheets at 400$^0$C***

Figures 4.22 and 4.23 above show the thickness distribution of the different blanks from one end of a sheet along the major strain direction and normal to the necking region for sheets at room temperature and annealed sheets at 400$^0$C in 45$^0$ orientation respectively. Comparison between curves of sheets at room temperature at Fig 4.22 with annealed sheet at 400$^0$C in the Fig 4.23, indicates the uneven thickness distribution for non-heat-treated curves of blanks with different size. A blank with 175x200mm has lager thickness distribution in centre of punch diameter, but in case of annealed sheet curve uniform thickness distribution observed. In general at the same punch force, the sheets room temperature have less thickness distribution than annealed sheets at 400$^0$C at 45$^0$ orientation

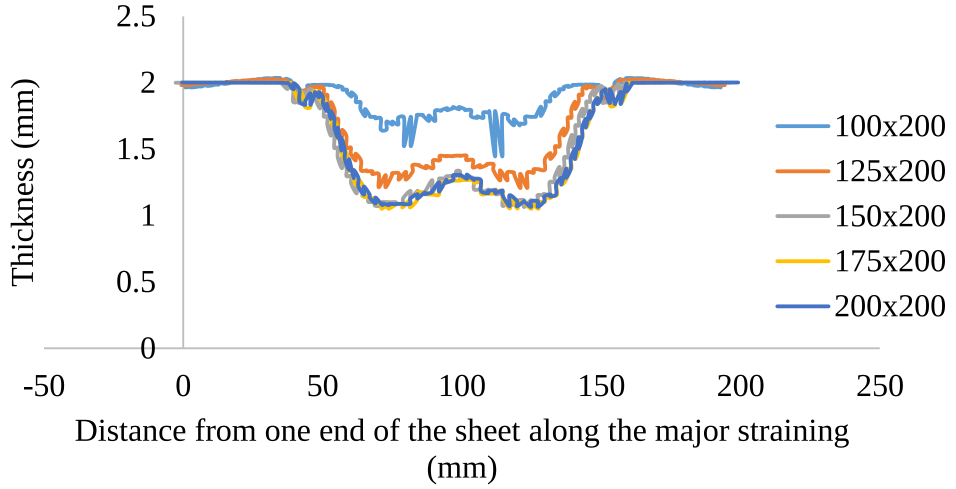


***Figure 4.24 Thickness distribution of 90$^0$ oriented sheets at room temperature***

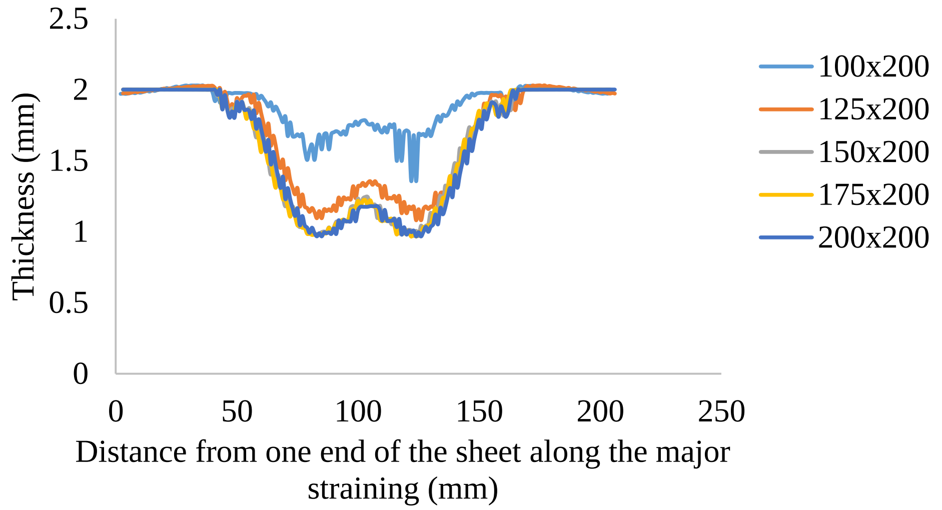


***Figure 4.25 Thickness distribution of 0$^0$ oriented annealed sheets at 400$^0$C***

Figures 4.24 and 4.25 above show the thickness distribution of the different blanks from one end of a sheet along the major strain direction and normal to the necking region at room temperature and after annealing process for 90$^0$ oriented sheets respectively. From the observation of the curves between sheets at room temperature at Fig 4.24 with annealed sheets at 400$^0$C in the Fig 4.25, indicates there is this difference in thickness distribution. The frequency of curves are smother for annealed sheet.

## 4.9 Evaluation of form limit diagram

The form limit diagram indicates the stretch formability characteristics of the sheet metal. The forming limit diagram is also the forming limit curve, which is one of necessary value during practical assessment of sheet stretch forming process. Figures 4.26 and 4.27 show the comparison between the form limit curves of AA6023 T-6 alloy sheets at room temperature and annealed alloy sheets and Table 4.6 indicate major and minor strain obtained by thickness gradient based necking criterion at LDH.

Table 4.6 Major and minor strain at LDH for room temperature blanks

| | $0^0$ oriented | | | | | $45^0$ oriented | | | | | $90^0$ oriented | | | | |
|---|---|---|---|---|---|---|---|---|---|---|---|---|---|---|---|
| Blanks | 1 | 2 | 3 | 4 | 5 | 1 | 2 | 3 | 4 | 5 | 1 | 2 | 3 | 4 | 5 |
| Major strain | 0.12 | 0.25 | 0.30 | 0.30 | 0.35 | 0.13 | 0.29 | 0.35 | 0.28 | 0.28 | 0.13 | 0.24 | 0.56 | 0.20 | 0.28 |
| Minor strain | 0.11 | 0.23 | 0.28 | 0.28 | 0.32 | 0.12 | 0.27 | 0.33 | 0.27 | 0.26 | 0.12 | 0.22 | 0.33 | 0.19 | 0.25 |
| LDH | 26 | 37.2 | 39 | 39 | 39 | 29.5 | 38.5 | 39 | 39.5 | 39.5 | 32 | 39 | 39.5 | 39.5 | 39 |

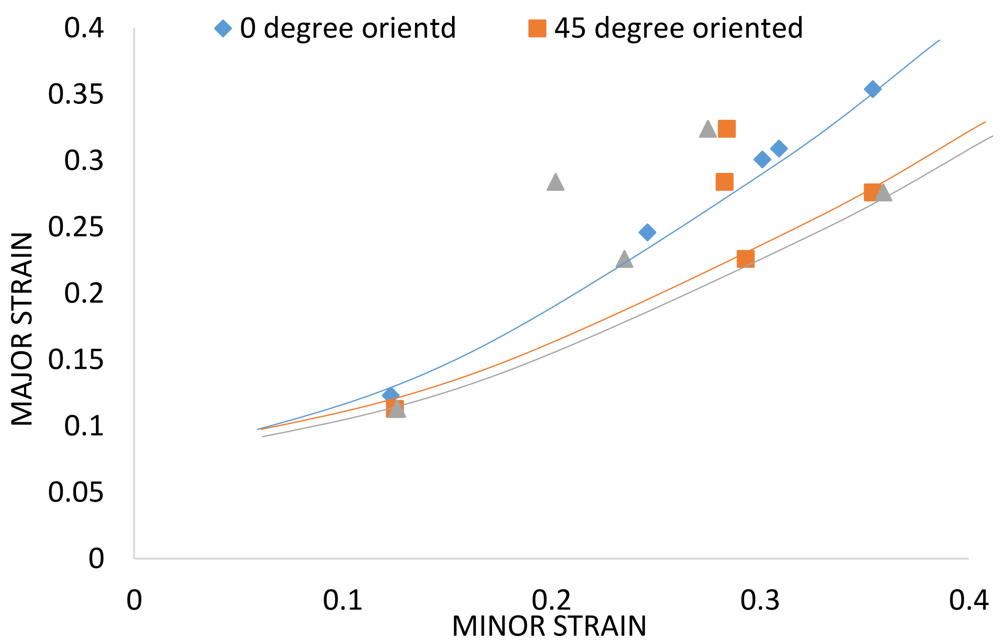


***Figure 4.26 Form limit curve of AA6023-T6 alloy sheet at room temperature forming condition***

Figure 4.26 show the form limit curves of a sheet that predicts the stretch formability of AA6023-T6 alloy sheet at room temperature. The distribution of the curves of blanks with different dimension to the upper limit curve ULC are scattered. There is some blanks lie above the upper limit curve ULC which indicates fracture before the necking. The stretch formability of these blanks which have fracture earlier than the forming limit are not acceptable. The earlier formation of fracture caused do to the cold forming condition. The maximum limit dome height LDH observed in the stretch formability of blanks under room temperature forming condition for blanks with dimension of 150x200, 175x200 and 200x200 is 39.5 mm. From the value of maximum limit dome height LDH, these blanks have good formability compared to the others blanks with minimum value of limit dome height. Table 4.7 indicate major and minor strain obtained by thickness gradient based necking criterion at LDH for annealed blanks.

Table 4.7 Major and minor strain at LDH for annealed blanks

| | $0^0$ oriented | | | | | $45^0$ oriented | | | | | $90^0$ oriented | | | | |
|---|---|---|---|---|---|---|---|---|---|---|---|---|---|---|---|
| Blanks | 1 | 2 | 3 | 4 | 5 | 1 | 2 | 3 | 4 | 5 | 1 | 2 | 3 | 4 | 5 |
| Major strain | 0.20 | 0.34 | 0.40 | 0.43 | 0.41 | 0.15 | 0.25 | 0.33 | 0.36 | 0.42 | 0.34 | 0.31 | 0.36 | 0.43 | 0.44 |
| Minor strain | 0.19 | 0.30 | 0.37 | 0.39 | 0.38 | 0.13 | 0.23 | 0.29 | 0.33 | 0.38 | 0.22 | 0.28 | 0.33 | 0.39 | 0.40 |
| LDH | 31 | 40.5 | 41.5 | 42 | 41.5 | 32 | 42.5 | 43 | 43 | 43 | 30.5 | 41.5 | 43 | 43 | 43 |

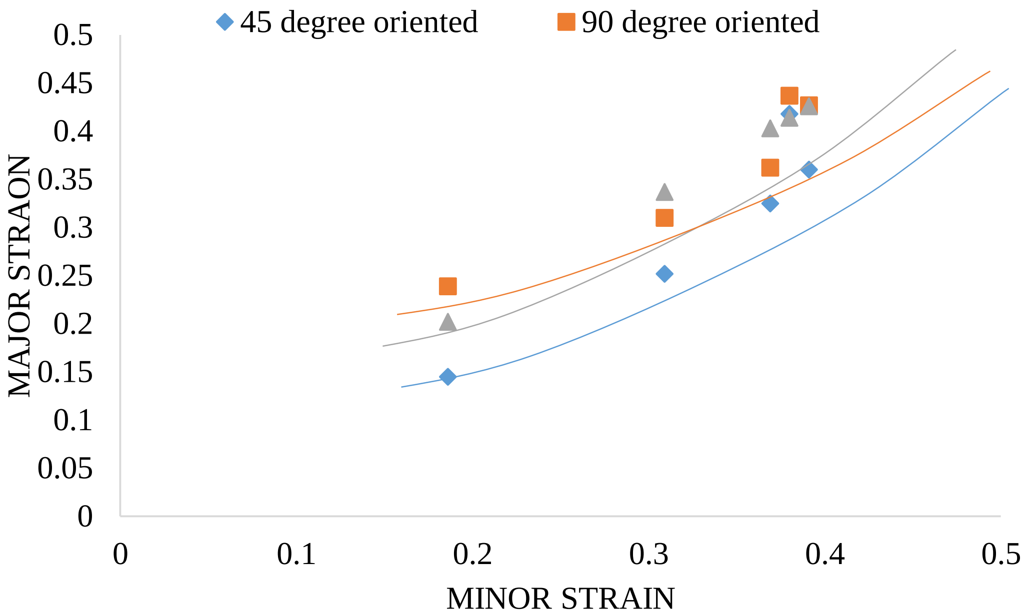


***Figure 4.27 Form limit curve of AA6023-T6 alloy sheet after annealing condition***

Figure 4.27 shows the form limit curves of sheet that predicts the stretch formability of annealed AA6023- T6 alloy sheet. The distribution of the curves of blanks with different dimension to the upper limit curve ULC are scattered. The distribution of the curves of the blanks are under limit of the upper forming limit diagram. This indicates there is no earlier fracture occurred before necking. The stretch formability of these blanks which are scattered blow the upper forming limit curve UFLC and near to the upper limit curve are recommended blanks for attaining a good formability. The maximum limit dome height LDH observed in the stretch formability of blank which are formed after annealing condition with dimension of 150x200, 175x200 and 200x200 is 43. From the value of maximum limit dome height LDH, these blanks have good formability compared to the others blanks with minimum value of limit dome height. The comparison between the maximum limit dome heights of the blanks at room temperature annealed alloy sheet shows the stretch formability of AA6023-T6 alloy sheets. The average maximum limit dome height LDH for room temperature forming condition of the blanks is 39.5mm and the average maximum limit dome height LDH is 43mm. Therefore, annealed AA6023-T6 alloy sheet has a good formability at annealing temperature of $400^0$C and 90 minutes soaking time than sheet at room temperature.

# CHPTER 5

## CONICLUSIONS AND FUTURE SCOPE

### 5.1 Conclusions

From the present work the following conclusions are drawn.

1. There is refined microstructure observed for annealed at $400^0$C sample compared to sheet at room temperature. Annealing process of AA6023-T6 alloy sheet did not affect the microstructure rather than improving.
2. Annealing process caused the change in hardness of the AA6023-T6 alloy sheet. For 10 kg load of test average reduction in HV is 23 and for 5 kg is 17. The average percentage of reduction in HV is 0.2 % which is acceptable value for application of sheet.
3. The thickness distribution of the blanks at room temperature compared to thickness distribution of annealed blanks at $400^0$C from one end of a sheet along the major strain direction and normal to the necking region. Therefore, annealed AA6023-T6 alloy sheets at $400^0$C has good stretch formability.
4. LDH from simulation justified the stretch formability behaviour of AA6023 –T6 alloy sheet. A blank at room temperature with dimensions of 150x200, 175x200 and 200x200 have 39.5mm maximum dome height and blank with dimension of 100x200 and 125x200 at room temperature have 26mm minimum dome height.
5. Annealed blanks at $400^0$C with 150x200, 175x200 and 200x200 dimensions have maximum dome height compared to 100x200 and 125x200 blanks at room temperature. The maximum dome height observed in simulation is 43mm and minimum 31mm. By which, the blanks with dimension of 150x200, 175x200 and 200x200 have good stretch formability compared to blanks with dimension of 100x200 and 125x200 at room temperature.
6. The comparison between stretch formability of AA6023-T6 alloy sheet at room temperature and annealed sheet at $400^0$C shows, AA6023-T6 alloy sheet at room temperature has 39.5mm maximum dome height and annealed sheet at $400^0$C has 43mm maximum LDH, therefore, annealed sheet has good stretch formability.

## 5.2 Future Scope

1. Conducting experimental work for stretch formability and compering with simulated results can better explain the stretch formability.
2. Different annealing temperature can be used to get better stretch formability
3. Modern industries like: automotive, aircraft and aerospace can use the results obtained from this study to get better stretch formability
4. Different forming speed can be used to obtain better stretch formability
5. Optimization of forming parameter can be used to gate better stretch formability of sheet metals

## REFERENCES


[1]. Stanislav Nemeth, Anna sunova, Emil Evin. (2013). Forming limit diagrams as an important indicator. *Transfer inovácií*, 26.

[2]. Yasumasa Chino, K. S. (2008). Tensile Properties and Stretch Formability of Mg-1.5 mass%-0.2 mass%Ce. *Materials Transactions, 49,* 171-1712.

[3]. W. J. Ali, O. T. (2012). Warm Forming of Aluminum Alloy 2024 at Different Temperatures. *Al-Rafidain Engineerin, 20*, 78-85.

[4]. Lange, K. (1985). *Handbook of metal forming.*

[5]. R.P.R. Cardosoa, O. A. (2017). A generalisation of the Hill's quadratic yield function for planar plastic. *International Journal of Mechanical Sciences, 128–129* , 253-263.

[6]. Aboozar Taherizadeh, D. E. (2011). Evaluation of advanced anisotropic models with mixed hardening. *International Journal of Plasticity, 27*, 1781–1802.

[7]. Mohamed, A. I. (2016). Review on sheet metal forming process of aluminium alloys. *Proceedings of the 17 MS 129 th Int. AMME Conference,, 19-21* , 129-141.

[8]. Artur Klosa, A. K. (2017). Experimental and numerical studies on the forming behavior of high. *17th International Conference on Sheet Metal, SHEMET17, 183*, 95 – 100.

[9]. Hidetoshi Somekawa, A. K. (2016). *MaterialsScience&EngineeringA, 676*, 427–433.

[10] .Tigran Abovyana, G. T. (2015). Formability prediction of aluminum sheet alloys under isothermal. *Journal of Manufacturing Processes, 20*, 406–413.

[11] R. A. Nolan, M.-A. K. (2013). The effect of temperature on the formability of a high strength aluminium automotive alloy. *University of Manchester (School of Materials, The University of Manchester, Oxford Road, Manchester, M13 9PL),* 1-8.

[12] Y. Tokitaa, T. N. (2017). Stretch formability of high strength steel sheets in warm forming. *Journal of Materials Processing Technology , 246*, 77-84.

[13]. W. J. Ali, O. T. (2012). Warm Forming of Aluminum Alloy 2024 at Different Temperatures. *Al-Rafidain Engineering, 2,* 78-85.

[14]. Yasumasa Chinoa, a. M. (2009). Enhanced stretch formability of Mg–Al–Zn alloy sheets rolled at high temperature (723 K). *Scripta Materialia, 60*, 447-450.

[15]. Xinsheng Huang, K. S. (2010). Influences of initial texture on microstructure and stretch formability of Mg–3Al–1Zn alloy sheet obtained by a combination of high temperature and subsequent warm rolling. *Scripta Materialia, 63,* 395-398.

[16]. B-A Behrens et al. (2017). Influences on the formability and mechanical properties of 7000-aluminum alloys in hot and warm forming. *36th IDDRG Conference – Materials Modelling and Testing for Sheet Metal Forming*, *896*, 1-8.

[17]. Zhu Chen, G. F.-Q. (2017). Formability Evaluation of Aluminum Alloy 6061-T6 Sheet. *Journal of Materials Engineering and Performance at Room and Elevated Temperatures, 26,* 426-4637.

[18]. WANG Hui, L. Y.-b.-h. (2012). Warm forming behavior of high strength aluminum alloy AA7075. *Trans. Nonferrous Met. Soc. China, 22*, 107.

[19]. D Raja Satish, D. R. (2017). Effect of temperature and punch speed on forming limit strains of AA5182 alloy in warm forming and improvement in failure prediction in finite element analysis: A case study. *Journal of Strain Analysis, 52*(4), 258-273.

[20]. Yasumasa Chino, X. H. (2010). Enhancement of Stretch Formability at Room Temperature by Addition of Ca in Mg-Zn Alloy. *Materials Transactions, 51*, 818 - 821.

[21]. Kazutaka Suzuki, Y. C. (2015). Enhanced Room-Temperature Stretch Formability of Mg0.2 of High-Temperature Pre-Annealing and Warm Rolling. *Materials Transactions, 56*, 1096 - 1101.

[22]. Yasumasa Chino, K. S. (2008). Texture and Stretch Formability of Mg-1.5 mass%Zn-0.2 mass%Ce Alloy Rolled at Different Rolling Temperatures. *Materials Transactions, 49*, 2916 - 2918.

[23]. Rongshi Chen, S. L. (2012). Consideration of Castability and Formability for New Magnesium Alloys. *Open Journal of Metal, 2*, 8-17.

[24]. Y.G. An. (2001). Strain path change effects on stretch formability of 6082 aluminium alloy. *Materials Science and Technology, 17*, 258-263.

[25]. Tao Zhou, Z. Y. (2015). Effect of the final rolling speeds on the stretch formability of AZ31 alloy sheet rolled at a high temperature. *Journal of Alloys and Compounds*, *650*, 436-443.

[26]. Keeler, S. (1965). Determination of forming limits in automotive stamping sheet metal. *42*, pp. 683-690.

[27]. Goodwin, G. (1968). Application of strain analsis to sheet metal forming problems in the press shop. *SAE Trains, 77*, 380-387.

[28]. Sreenath D Kumara, A. T. (20016). Forming Limit Diagram Generation of Aluminum Alloy AA2014 Using Nakazima Test Simulation Tool. *International Conference on Emerging Trends in Engineering, Science and Technology ICETEST, 24,* 386 – 393.

[29]. M. Aghaie-Khafri. (2004). Formability of AA8011 aluminum alloy sheet in homogenized and unhomogenized conditions. *Journal of materials science, 39*, 6467-6472.

[30]. Ryoichi Chiba, H. T. (2015). Forming-limit prediction of perforated aluminium sheets with square holes. *Journal of Strain Analysis, 56*(6), 391-404.

[31]. A. Martinez Lopez, a. A. (n.d.). Forming limit curves under stretch - bending. *Materials inovation institute*.

[32]. Z. Shao, Q. B. (2014). Experimental investigation of forming limit curves and deformation features in warm forming of an aluminium alloy. *University of Technology, Dalian*, 1-23.

[33]. Jan Bohlen, G. C. (2018). Processing Effects on the Formability of Magnesium alloy sheets. *Metals, 8*, 147.

[34]. Endre Romhanji, D. G. (2001). Forming aspects of high-strength al-mg. *materiali in tehnologije, 35*, 1-2.

[35] S. Bruschi, T. A. (2014). Testing and modelling of material behaviour and formability in sheet metal forming. *CIRP Annals - Manufacturing Technology, 63*, 727-749.

[36] D.H. Kang, D.-W. K. (2009). Relationship between stretch formability and work-hardening capacity of twin-roll cast Mg alloys at room temperature. *Scripta Materialia, 61*, 768-771.

[37] M. Sivanandini, D. S. (2012). Formability of Magnesium Alloys. *International Journal of Modern Engineering Research (IJMER), 2*(4), 2464-2471.

[38] Anoop Kumar. (2017). Influence of sheet metal thickness on formability of aluminium alloy 6061. *international journal of current engineering and scientific research (IJCESR), 4*, 2394-0697.

[39] K.Logesh, V. R. (2017). Experimental investigation on formability analysis, mechanical and corrosion behaviour of aa1100 sheet metal. *International Journal of Mechanical Engineering and Technology (IJMET), 8*(8), 900–909.

[40] SM Hussainia, S. K. (2015). Formability studies of ASS 316 under different forming conditions. *4th International Conference on Materials Processing and Characterization*, *2*, pp. 1987 – 1995.

[41]. K. Okazaki, M. K. (1980). Material parameters of importance in the stretch forming of ti-6al-4v sheet at 300-950 K. *Metallurgical Engineering and Materials Science Department,University of Kentucky, 2*, 864-871.

[42]. Marilena C. Butu, C. T. (2012). Analysis of sheet metal formability through isotropic and kinematic hardening models. *European Journal of Mechanics / A Solids, 30*(4), 532.

[43]. Dr.Sc. Amra Talić – Čikmiš, D. A.–Č. (2011). Experimental determination of forming limit diagram. *14th International Research/Expert Conference, 1*, 605-608.

[44]. J. Sota, E. S. (2005). Comparison of the fornig -limit diagram (FLD) model for drawing quality (DT) steel sheets. *Metalurgija, 44*, 449-255.

[45]. R. Raman Goud, K. P. (2014). Formability limit diagrams of extra-deep-drawing steel at elevated temperature. *3rd International Conference on Materials Processing and Characterisation*, *6* , 123 – 128.

[46]. M. Shakeri, B. D. (2001). Forming limit diagram of metal sheet in actual strain path with respect to forming process. *Transactions on Engineering Sciences, 32*, 154-161.

[47]. L. H. Martínez-Palmeth, A. J.-D.-L. (2013). Formability of Automotive H240LA Steel Sheets in Stretch–bending process. *The Manufacturing Engineering Society International Conference*, *63* , 669 – 677.

[48]. D.H. Kang, D.-W. K. (2009). Relationship between stretch formability and work-hardening capacity of twin-roll cast Mg alloys at room temperature. *61*, 768–771.

[49]. Holmberg, S. E. (2004). Evaluation of sheet metal formability by tensile tests. *Journal of materials processing technology, 145*(1), 72-83.

[50]. Chen, F. K. (2007). A formability index for the deep drawing of stainless steel rectangular cups. *The International Journal of Advanced Manufacturing Technology, 34(9-10),, 34*, 9-10.

[51]. D.M. Rodrigues, c. L. (2009). A multi-step analysis for determining admissible blank-hlder force in deep-drawing operation Materials and DEsign.

[52]. José Divo Bressan, J. C. (2010). A Numerical Simulation Study Of Deep Drawing Testing And Experimental Results Of Steel Sheets, Using a Commercial Software Int J Mater Form. *3*, 231-234.

[53]. Bagheriasl, R. (2012). Formability of aluminium alloy sheet at elevated temperature.

[54]. https://www.slidesh.net/sajeedmahoboob

[55]. P J Ramulu, R. G. (2011). Weld zone representation during the formability prediction of friction stir welded blanks with similar thickness sheets. *The Journal of Strain Analysis for Engineering Design*, *46*, 456-477.